

## **Appendix 4**

# **Spectral Reflectance of Whitecaps: Fractional Coverage and the Augmented Spectral Reflectance Contribution to Water-Leaving Radiance**

Karl D. Moore, Kenneth J. Voss, Howard R. Gordon

Physics Dept., University of Miami

Coral Gables, FL 33124

Submitted to *Journal of Geophysical Research*

**Abstract.** A radiometric system, deployed from a ship, is used to directly measure the optical influence of whitecaps. Estimates of the augmented reflectance contribution and fractional coverage are determined from measurements in the Gulf of Mexico and open ocean waters of the Pacific. The accuracy of these estimates are dependent on the ability to radiometrically determine the difference between white water and nonwhite water events. Subtle spectral variations in the visible are found in the augmented reflectance but are typically smaller than the error in determining the white water threshold. Sky reflectance, sky condition, specular sun glitter, wave height and wind direction can influence the spectral characteristics of the augmented reflectance particularly at low sun angles. Evidence is presented suggesting that whitecaps cannot be modeled as lambertian reflectors, particularly at low solar elevations. The augmented spectral reflectance of whitecaps measured in the open ocean is found to be 0.00031 at a wind speed of 8 m/s, 0.00058 at 10 m/s, and 0.00096 at 12 m/s for wavebands in the visible and 15% - 25% less at 860 nm.

## **Introduction**

Due to the relatively small water-leaving radiance signal from the ocean in comparison to the total light arriving at an ocean color sensor, the quality of data depends primarily on the accuracy of atmospheric correction algorithms. Atmospheric correction over the ocean is determined by measurement of the upwelling signal arriving at the satellite at a waveband where the radiance back scattered out of the ocean is known to contribute very little or no signal [*Gordon and Wang, 1994a*]. Utilization of near infrared wavebands beyond 760 nm (and even 670 nm) can be justified in the absence of whitecaps (in case I waters) due to the strong absorption properties of liquid water at those wavelengths. In the case of an agitated sea state the presence of whitecaps occurring within a satellite image pixel augments the radiometric signal by an amount dependent on the whitecap coverage and the reflectance of whitecap foam [*Gordon and Wang, 1994b*]. This is referred to as the augmented reflectance of whitecaps. Previous researchers have used a whitecap foam reflectance of 50% - 100% [*Payne, 1972; Maul and Gordon, 1975; Gordon and Jacobs,*

1977] and have assumed it to be constant at all wavelengths. Laboratory measurements carried out by *Whitlock et al.* [1982] yield a value of ~55% in the visible part of the spectrum for dense foam in clear water and have shown that it diminishes with increasing wavelength beyond ~0.8  $\mu\text{m}$ , with 5% decrease at 0.85  $\mu\text{m}$ , 10% at 1.02  $\mu\text{m}$ , and 50% at 1.65  $\mu\text{m}$ . *Koepke* [1984] determined the effective reflectance of whitecaps, which takes into consideration the decrease in reflectance and increase in area of an individual whitecap as it ages, to be 22% in the visible. This wavelength independent estimate of the effective reflectance is then combined with the relative area covered with whitecaps as a function of wind speed [*Monahan and O'Muircheartaigh*, 1980] in order to obtain the total optical influence of whitecaps for different wind speeds. *Koepke* found that it was necessary to introduce this value of effective reflectance since the simple combination of fractional coverage with the foam reflectance values of *Whitlock*, valid for dense fresh foam (~55%), gave too high a value for the optical influence of the total whitecap.

Field measurements taken of the reflectance of foam generated by breaking waves in the surf zone [*Frouin et al.*, 1996] indicate a larger spectral variation in reflectance than reported by *Whitlock*. *Frouin* found the reflectance decreased by 40% at 0.87  $\mu\text{m}$ , 50% at 1.02  $\mu\text{m}$ , and 95% at 1.65  $\mu\text{m}$  relative to the reflectance at 440 nm. The greater spectral variation in reflectance found in field data, unlike the laboratory foam of *Whitlock*, is thought to be due to the strong absorption properties of water at longer wavelength acting on light reflected from submerged bubbles forced into the water column by the breaking waves.

In addition to the spectral differences between foam measured in the laboratory and in the field, estimates of whitecap fractional coverage for different wind speeds are found to be quite noisy [*Blanchard*, 1971; *Monahan*, 1971; *Ross and Cardone*, 1974; *Wu*, 1979; *Toba and Chaen*, 1973; *Monahan and O'Muircheartaigh*, 1980,1986]. Fractional coverage ( $W$ ) has been typically related to wind speed ( $U$ ) with the form  $W = \alpha U^\beta$ . The values of  $\alpha$  and  $\beta$  vary with geographic location, air and sea temperature as well as wind speed range. These relationships remain noisy, despite attempts to fine tune particular data sets, due to the dynamic nature and interdependence of the many parameters involved in whitecap formation. Whitecap coverage is primarily dependent

on wind speed, but also on other factors such as fetch and duration [Cardone, 1969], water temperature [Miyake and Abe, 1948], air temperature, stability of the lower atmosphere defined by the air/water temperature differential [Monahan and O'Muircheartaigh, 1986], salinity [Monahan and Zietlow, 1969] and even surface tension variations due to the presence of organic films [Garrett, 1967]. A slightly different approach by Wu [1988] relates whitecap coverage to wind-friction velocity, being proportional to the square root of the wind stress which depends strongly on atmospheric stability conditions. Bortkovskii and Novak [1993] assessed whitecap and foam coverage with particular dependence on the sea surface temperature which effects sea water viscosity and wind friction.

In addition, defining a threshold between white water and nonwhite water events is a difficult process and usually depends on a subjective interpretation. Further complexities can arise, such as the increase in foam streak-to-whitecap ratio with wind speed above 9 m/s [Ross and Cardone, 1974]. As the foam streak approximates a single bubble layer with a low reflectance contribution that is close the threshold, a greater error can be induced in the estimate of the augmented reflectance contribution at higher wind speeds.

To date, the optical influence of whitecaps on the upwelling water-leaving radiance has been estimated by utilizing and combining the work of different researchers as described above. In this paper, a measurement system deployed from a ship is used to directly determine the augmented spectral reflectance and fractional coverage of whitecaps in the field. Our measurement system provides spectral reflectance data from individual whitecaps - as they grow and decay - and, by integrating over longer periods of time, estimates of the fractional coverage and augmented reflectance contribution to the water-leaving radiance can be determined. The principal reason we undertook the present investigation was to see if the Frouin *et al.* [1996] spectral measurements in the surf zone were applicable to real oceanic whitecaps. A secondary motivation was to validate the whitecap reflectance versus wind speed relationship proposed by Koepke [1984] [Gordon and Wang 1994b].

## **Instrument System**

The whitecap reflectance measurement system is described in detail elsewhere [Moore *et al.*, 1997]. The system consists of a 6-channel radiometer with narrow field of view and nominal 10 nm bandpasses at 410, 440, 510, 550, 670 and 860 nm. It is held over the water surface by means of a boom extended from the bow of a ship providing an unobstructed view of the water surface. At the same time a cosine collector with matching wavebands measures downwelling irradiance so that the reflectance of the water surface can be calculated. A TV camera is mounted by the radiometer to provide a visual reference, and whenever the radiometric data is acquired the associated video frame is time and date marked and recorded onto video tape to assist in later analysis. Air and water temperature, wind speed and direction are measured simultaneously with the radiometric data at a rate of ~7 times a second continuously for about 30 seconds (providing 200 contiguous samples), after which global positioning (GPS) data, universal time, and location are recorded. This acquisition sequence is repeated until a time determined by the operator. This radiometric rate allows many sample points of an individual whitecap to be captured as well as providing an adequate data set over a time period of reasonably consistent sea state and sky conditions.

Once the system has been installed on a ship, only periodic measurements of the dark current are required. This requires bringing the radiometer in from the boom and covering both the radiometer and the deck cell with light tight caps. This is necessary only when significant temperature changes are encountered such as when conditions change from early morning to noon, or from dark, overcast, rainy conditions to bright sunshine. The radiometer can also be angled up to 20° from nadir in order to minimize the effects of specular sun glitter and bright sky reflections.

## **Data Description**

Data from two different cruises are presented in this paper. The data acquired from the first cruise is used to introduce the data reduction process, consider the difficulties in radiometrically defining white water events and to investigate the effects that low solar elevation, wind direction,

specular sun reflection and sky conditions have on the estimate of fractional coverage and on the augmented spectral reflectance contribution. In the second cruise, data was acquired in the open ocean and is used to provide practical measurements of the augmented reflectance contribution needed for ocean color and atmospheric correction algorithms.

For the first cruise, the whitecap radiometer system was deployed in the spring of 1996 on the NOAA ship, R/V Malcolm Baldrige for a 21-day ship cruise from Miami to a test location in the Gulf of Mexico, approximately 70 miles offshore from Cedar Key (Florida) in the Apalachicola Bay. The location provided relatively warm waters ( $\sim 16 - 17^{\circ}\text{C}$ ) with a number of cold fronts moving down off the continental mainland, resulting in variable conditions. These fronts usually lasted a couple of days bringing strong winds (sometimes as high as 18 m/s) and lowering the air temperature to about  $12^{\circ}\text{C}$ . The occurrence of an unstable atmosphere and good winds provided an interesting whitecap data set.

The second cruise involved a  $\sim 6,000$  km transit through equatorial waters of the Pacific Ocean from Manzanillo, Mexico to Honolulu, Hawaii. This 13-day cruise took place in November 1996 aboard the NOAA ship R/V Ka'imimoana. Conditions were more consistent with air/water temperature and wind speed/direction changing only by a relatively small amount over time. Fetch was typically greater than 1000 km and duration could be considered unlimited. Data was acquired far from land and for the most part, water temperature was  $\sim 22-23^{\circ}\text{C}$  with air temperature  $\sim 20-23^{\circ}\text{C}$ . Wind speeds ranged from  $\sim 8$  m/s to  $\sim 13$  m/s and wind direction changed from an initial northerly direction at the beginning of the transect to an easterly and southerly direction as the Trade winds were crossed. The sky conditions were mainly broken and scattered with some overcast periods.

The data used in the following section was acquired during one particular cold front passage during the first cruise in the Gulf of Mexico. The front approached in the morning with a completely overcast sky. Wind speed was initially  $\sim 6$  m/s from the south east but at about 10:40 am the wind changed direction to the north northwest with wind speed increasing to about 15 m/s (gusting to 18 m/s) within 15 minutes. The water surface which had been relatively 'flat' with a

wave height of about 1-2 ft (30 - 60 cm) became ruffled with many small whitecaps appearing. As the day progressed the whitecaps became larger but fewer in number as the wave height increased and a swell began to develop. Although there were lull periods, the winds picked up again during the night blowing between 10 to 15 m/s and changing direction to the east as the front passed. By the next day, the wave height had increased to 2 m with a swell frequency of 7-8 seconds. The sky was clear and the ship adopted a rocking motion with the sea swell. Examples of data taken from both days with similar wind speeds but differing sea states, sky conditions, air temperatures, duration, etc. are presented in the next section.

## **Data Reduction**

### **Phase I Reduction Process**

One half hour of data collected at the rate described above amounts to about a 1.5 megabytes of data storage. To reduce this data, analysis software using Matlab was developed to partition and separate the data matrix into radiometric data, environmental parameters (wind speed/direction, air/water temperature) and GPS data. The radiometric data is then reduced to produce dark background-subtracted and radiometrically-corrected reflectance values from the six up- and downwelling channels. This radiometric correction process consists of three steps [Moore *et al.*, 1997] briefly reviewed here.

First, ratios of upwelling radiance to downwelling irradiance are formed from the dark subtracted signals for each channel. These six ratios are then multiplied by a calibration factor determined in the laboratory relating the channels in the radiometer to those in the deck cell in order to yield reflectance measurements. This was established using a calibrated 1000W (FEL) quartz halogen lamp source and a calibrated Spectralon reflectance plaque. The deck cell was positioned 50 cm in front of the source and measurements taken. For the radiometer, the reflectance plaque replaced the deck cell, and the radiometer viewed the plaque from a 45° angle.

For the second step, a multiplication factor is required to correct bandpass differences between the radiometer and deck cell and for differences in the light spectrum between laboratory and outdoor illumination conditions.

Thirdly, each channel of the deck cell must be corrected for solid angle response for operation outdoors under  $2\pi$  illumination due to the slight deviation in angular response of the deck cell cosine collector from true cosine. Correction factors for different angular distributions of the downwelling light field are required for various sky conditions that may be encountered. A set of correction factors were established for different sky conditions such as overcast, or clear sky with different solar zenith angles, to correct solid angle response.

After applying these corrections, the corrected data are presented as a time series in blocks of 200 water surface reflectance measurements along with wind speed/direction, air/water temperature, upwelling radiance and downwelling irradiance data. The reflectance data are then grouped into reflectance intervals; any reflectance spectra whose average value falls within a predetermined reflectance interval is binned. In analysis of foam data obtained with the system in earlier work [Moore *et al.*, 1997], the value of the reflectance at 860 nm was used as the binning parameter rather than the mean spectral value used here. However, in estimating the fractional coverage and augmented spectral reflectance, it was found that it makes no difference which parameter is used.

For analysis of the data from the first cruise, the reflectances are divided into 48 intervals, with high resolution reflectance intervals of 0.0025 reserved for reflectance values between 0.005 and 0.1. (First interval is 0.0 to 0.005). Above this, the reflectance intervals are incremented by 0.1 and continue up to 1.0. As will be seen later, the high resolution intervals used for the lower reflectance values below 0.1 have been implemented in an attempt to accurately determine and discriminate between white water and nonwhite water events. Reflectance intervals above 0.1 were primarily used to analyze the spectral characteristics of different foam types which may be defined by their reflectance magnitude.

In the work by *Frouin et al.* [1996] in making spectral measurements of foam in the surf zone, reflectance intervals were also used in an attempt to determine spectral variations with foam type and thickness. The total reflectance was partitioned into 4 intervals (0 - 0.25, 0.25 - 0.4, 0.4 - 0.55, and any reflectance greater than 0.55). *Koepke* [1984] on the other hand required a threshold between nonwhite water and white water in analysis of photographic images to determine fractional coverage and the effective reflectance, which considers the drop in reflectance and increase in area as a whitecap decays. To accomplish this, the white water threshold was set at 0.1 with the maximum reflectance in a particular photograph normalized to 1. These images were acquired using a 6 cm x 6 cm Hasselbad camera angled between 45° and 60° degrees in viewing the surface from a height of 30 m. This threshold was further complicated by the increased white threshold towards the horizon due to increased Fresnel sky reflection. With the whitecap radiometer used in this paper, the effect of sky reflection variation with viewing angle is drastically reduced due to the small field of view of the radiometer optics (1°), and with 0.0025 reflectance resolution more accurate threshold information can be obtained.

After the reflectance data from each block has been grouped into reflectance intervals, these reflectance intervals are added to previous blocks of similarly reduced reflectance data, resulting in a set of reflectance intervals for the complete data matrix. UTC time is extracted and displayed at the beginning of each block so that reflectance measurements can be correlated with water surface events replayed on the VCR. The VCR (Sony EV-C100 (video Hi8)) can be advanced frame by frame in either direction with the time/date mark appearing on the bottom of the monitor approximately every third frame. In this way, individual samples from whitecaps and their different foam types can be radiometrically tracked.

Once all the data from a particular acquisition period has been reduced to this level, the spectral reflectance values and the number of samples binned in each interval are stored along with the total number of samples taken, mean air/water temperature, wind speed/direction readings and GPS data from each block (200 samples) of the original data matrix.

## Phase I Examples

In Fig. 1(a) an example of a time series with two whitecaps passing under the radiometer is shown. These whitecaps were acquired during the onset of the cold front described above. The sky was overcast and the data were taken ~11:00 am. Wind speed was ~12 m/s, air temperature 16.2°C and water temperature 17°C. The 96 samples (from a block of 200) shown in Fig. 1(a) were acquired over a period of ~15 seconds. In this example, a large whitecap suddenly breaks into view of the radiometer with thick white foam (sample point 11) reaching a peak reflectance of ~55%. Six traces are plotted representing the six radiometer channels (410, 440, 510, 550, 670 and 860 nm). The lower trace (symbols) corresponds to the 860 nm reflectance. Thick foam is temporarily replaced by a region of submerged bubbles and thinner surface foam (~sample points 13, 14, 15). Thick foam comes into view again at sample point 17. At sample point 20 and 21 a thin layer of foam passes followed by some dense (not thick) older foam and stays in field of view to about sample point 35. Sample points from about 35 - 56 show the reflectance of thinning residual and fragmented surface foam. From 60 to about 75 the reflectance of the foam free water surface is shown and is suddenly followed by another whitecap of smaller magnitude (sample point 76) which continues to decay out to about sample point 96.

In Fig. 1(b) the individual reflectance samples from this sample period have been binned into reflectance intervals. The lower reflectance intervals correspond to the nonwhite water reflectance; some are higher due to Fresnel reflectance from brighter regions of the sky, others are lower due to shadowing by adjacent waves. The variation in the spectral profiles of each interval is partly due to the small number of samples used. However, a common feature that stands out is the lower 860 nm reflectance. This is attributed to reflectance from submerged bubbles modified by the strong absorption of water at 860 nm [Frouin *et al.*, 1996; Moore *et al.*, 1997]. (Other examples of phase I data reduction into reflectance levels are shown in Figs. 2(b), 3(b) and 4(b) where larger data sets of about 10,000 samples are used).

## **Phase II Reduction Process**

In phase II, the reduced data from phase I are processed to determine fractional coverage and the augmented spectral reflectance contribution. Correlations between these estimates and the environmental conditions responsible for whitecap development can then be investigated.

Each reflectance interval, resulting from the reduction of a complete data matrix, is multiplied by the fraction of reflectance samples that have contributed to that reflectance interval. This weighted reflectance spectrum is the effective spectral reflectance contribution of that reflectance interval (i.e. the contribution of that interval to the total reflectance). Repeating this for all reflectance intervals and summing their effective reflectances together yields the total spectral reflectance. This is equivalent to the reflectance observed in a satellite image pixel mapped onto the ocean surface.

The total reflectance contains both white water and nonwhite water contributions. In order to determine only the contribution of whitecaps and foam, the background water-leaving radiance, sky reflectance, sun glitter and other nonwhite water contributions must be removed. The background water color (and sky reflection etc.) has the greatest number of samples being the most frequently measured and since the presence of foam on the surface of the water increases the overall reflectance signal, the optimal threshold must be at some reflectance interval above it. However, reflectance intervals above the reflectance interval with the most number of samples may contain both thin foam reflectance as well as sky reflectance contributions from brighter regions of the sky. Also, reflectance intervals below this may contain thin foam reflectance contributions that are in the shadow of an adjacent wave and may register as having a lower reflectance than a sky reflectance contribution from an unshadowed foam free water facet. This is true for threshold intervals near the reflectance interval with the most number of samples. This inability to distinguish between white water and nonwhite water events places a limit on the accuracy with which fractional coverage and augmented spectral reflectance contribution can be determined.

The estimate of fractional coverage and the augmented reflectance contribution is dependent on choosing a reasonable reflectance threshold. Once an appropriate threshold has been chosen, it

is subtracted from each interval above it. This difference in reflectance is assumed to be due to white water contributions only. The reflectance difference is then multiplied by the fraction of samples that have fallen into that reflectance interval to yield the effective augmented spectral reflectance of that particular reflectance interval. All the weighted reflectance intervals above the threshold are summed to yield the (total) augmented spectral reflectance contribution. Fractional coverage is estimated from the total number of white water samples divided by the total number of samples and, notably, is not weighted by the magnitude of reflectance.

In the following examples, a range of plausible thresholds are implemented to demonstrate the effects on the estimate of both fractional coverage and the augmented spectral reflectance contribution from data acquired with similar wind speeds but under different sky conditions, solar zenith angles, and sea states.

## **Phase II examples**

### **Overcast Sky**

Data presented in Figs. 2(a) - 2(d) were the result of 9,000 surface reflectance measurements acquired over a period of ~23 minutes as the ship covered a 4 kilometer path during the onset of the cold front described above. Mean location was 29.05°N and 83.51°W. During acquisition the mean wind speed was 11.86 m/s with a standard deviation of 3.6 m/s (gusts up to 18 m/s). The wind was from the north between 350° and 0°. Ship heading was originally ~170° during the first half of the acquisition period and then passed through a southerly direction and settled on a north westerly direction of 330°. The radiometer was nadir viewing and since conditions were overcast there was no specular sun glitter. Air temperature was 16.2°C and water temperature 17.0°C, resulting in a slightly unstable atmosphere. Other parameters taken from the ship's log were salinity (35.027 ppt), barometric pressure (1015.4 mB), and relative humidity (93%). In this example, during the onset of the cold front, many small whitecaps suddenly appeared on the relatively flat and dark water surface. Duration was limited to ~15 minutes with whitecap development and sea state measured during an abrupt transition period in weather conditions. The

resulting measurements produced high values of the augmented reflectance and fractional coverage estimates.

In Figs. 2(a) - 2(d) the more interesting portions of the output of data processed in phase II are presented. Figure 2(a) shows all the reflectance samples reduced to reflectance intervals. In Fig. 2(b) a histogram of the number of samples used to determine each reflectance interval is shown. Remember that the first 39 levels cover the mean reflectance spectral values between 0 and 0.1. Above that the reflectance intervals are incremented in 0.1 steps causing the bump at interval 40. In the histogram there seems to be no obvious distinguishing feature to identify the background from the white water, but as mentioned above, a suitable threshold must be above the reflectance interval with the most number of samples.

Figure 2(c) shows the total reflectance. The total reflectance spectrum peaks at 510 nm suggesting a blue-green color and a maximum value of  $\sim 0.06180$ . The nonzero value at 860 nm (0.02412) is mainly due to the overcast sky being reflected at the water surface. The graphs in Fig. 2(d) show the augmented spectral reflectance contribution and an estimate of the fractional coverage for different thresholds choices.

In Fig. 2(d) a range of reflectance intervals (intervals 16 through 23 and where interval 16 contains the greatest number of samples) are used as threshold reflectance intervals between white water and nonwhite water events. In the resulting estimates of the augmented spectral reflectance, the spectral shape has changed from that of the total reflectance. The spectral shape of the augmented reflectance seems to vary somewhat from one choice of threshold interval to another with exception of a common lower 860 nm value and a relatively flat region between 440 and 670 nm. The 860 nm value, as seen in previous data, is much lower than the other wavelengths.

For threshold intervals 16, 17 and 18 the fractional coverage estimates are particularly high (37.2%, 22.5% and 14.3%) for this wind speed of 11.86 m/s. From threshold interval 19 through 23, the spectral shape has become more settled and appears to be relatively constant with the exception of the 410 nm channel which appears to decrease with increasing threshold with respect to the other spectral values. In this range of thresholds, the estimates of fractional coverage are

also more plausible (9.5%, 6.9%, 5.3%, 4.1% and 3.7%). This spectral shape continues for higher threshold intervals (not shown here) and eventually breaks down with the highest threshold intervals due to a small number of samples.

It is interesting to note that the augmented spectral reflectance for these threshold intervals (19 through 23) maintain a small peak at 510 nm although it decreases with increasing threshold. Increasing the threshold moves the analysis into higher reflectance levels and therefore into thicker whitecap foam types. Investigation of the spectral variation of different foam types with increasing reflectance [Moore *et al.*, 1997] revealed a similar trend with the 510 nm value decreasing while the 670 nm and 860 nm values increased. The 410 nm value was also observed to decrease in the foam spectra.

The 510 nm reflectance maintains the highest value and is reminiscent of the total reflectance spectrum which is predominantly comprised of non-foam water reflectance contributions. The reflectance values of the wavebands in the visible region tend to equalize with higher threshold choice. The augmented reflectance spectral profiles seem reasonable and explain the apparent whiteness of whitecaps, where the channels covering the visible region are essentially equivalent with an increasing hint of blue-green for lower reflectance intervals. This is similar to what is visually observed; white thick fresh foam and blue-green thin foam where the background water color penetrates through the thin bubble layers.

With a consistent spectral profile for the higher threshold intervals, the optimal choice becomes difficult. However, it seems that threshold interval 23 is perhaps too far into the white water realm and can be ruled out as the optimum threshold choice. Threshold interval 19 might be a reasonable choice but could contain some non-foam bright sky reflectance contributions. It also has a particularly high 410 nm value that is not present when higher threshold reflectance intervals are applied suggesting the presence of some non-foam contributions. Being conservative, the optimal choice seems to be around threshold interval 20 or even 21. The augmented reflectances are 0.00315 and 0.00290 at 510 nm and 0.00169 and 0.00161 at 860 nm for thresholds 20 and 21 respectively. The fractional coverage estimates using these thresholds,

although a little high due to the inclusion of the thinnest foam types, are 6.9% and 5.3% respectively.

In the augmented spectra for thresholds 20 and 21, changing the threshold by a small reflectance of 0.0025 changes the fractional coverage estimate by 1.6% but only by  $-0.000186$  for the augmented reflectance in the visible (410 nm -550 nm), and by  $-0.00008$  for the augmented reflectance at 860 nm.

The upwelling signal, particularly in the lower threshold regions, is mixed with contributions from brighter sky reflectances, thin foam layers and fragmented foam patches. As stated before, there is no decisive definition of threshold; only a compromise between either obtaining a reasonably pure white water spectrum and underestimating the augmented reflectance contribution, or obtaining perhaps a more complete measure of the augmented reflectance contribution at the cost of including some nonwhite water contributions. It is important to include the lowest reflecting and thinnest foam types since they persevere longer than the thicker and more highly reflective foam and as result have great statistical weight in contributing to the total augmented reflectance. This threshold problem makes accurate determination difficult and somewhat subjective. However, it is comforting that the augmented reflectance is a weak function of the actual choice of the threshold.

### **Clear Sky**

In the next example, whitecap data was taken the next day (~9:05 am) under clear sky conditions, and as described above, with a more developed sea. Wave height was about 2 m with a periodicity of 7-8 seconds. Mean wind speed was 11.7 m/s with a standard deviation of 1 m/s coming from the north west at about  $340^\circ$ . The ship heading was  $355^\circ$  and moving through the water at 7 knots (2.6 m/s) covering a straight track of 4.3 km. Air temperature was  $12^\circ\text{C}$  and the water surface temperature was  $16.5^\circ\text{C}$ , resulting in an unstable atmosphere. Other parameters taken from the ship's log were salinity (35.0895 ppt), barometric pressure (1019.9 mB) and relative humidity (61%). This location ( $\sim 29.15^\circ\text{N}$ ,  $84.02^\circ\text{W}$ ) was approximately 20 km north and 56 km west of the location where the data during overcast conditions in Fig. 2 was acquired. With

wind speed continually blowing in the 10-15 m/s range for roughly a 24 hour period, the sea had become more fully developed, producing a different whitecap morphology and foam distribution from the previous day. Reflectance measurements included a larger proportion of foam streaks and residual foam patches resulting from larger breaking waves although less frequent than in the previous 'overcast' case.

In Fig. 3(a) the reflectance measurements reduced to reflectance intervals are shown and the histogram of reflectance interval vs. number of samples is shown in Fig. 3(b). Noticeable differences from the overcast sky condition are (i) the tighter distribution of samples about the peak, and (ii) the much lower sky reflectance ( $\sim 0.00276$  at 860 nm). This is the result of a low sun angle ( $30^\circ$  above the horizon) and the viewing angle of the radiometer. The radiometer was orientated to view the water surface at  $20^\circ$  from nadir in a direction opposite the sun in order to minimize specular sun glitter in the measurements. As a result, the sky reflectance signal arriving at the radiometer was from a region of the sky centered roughly  $80^\circ$  from the sun where the sky is dark relative to overcast conditions.

With regard to the histogram of reflectance interval vs. number of samples, it may be tempting to fit a symmetrical distribution about the mode and use the difference between the fit and the histogram to identify any augmentation. But this would assume an equal probability of darker and brighter sky reflectances contributing to the distribution from a symmetrical distribution of wave orientations of the water surface reflecting a proportionately graded sky. It is not that simple since the wind typically blows from one direction causing the waves to progress across the surface in rows creating a preference for surface angle orientation and skewing any symmetry in the distribution. In addition, in the presence of low sun angles, the distribution of reflectance intervals is further complicated by the specific illumination direction of the sun reflected from waves and whitecaps. Even if the distribution of reflectance intervals vs. number of samples were perfectly symmetric, the finite bandwidth of this distribution indicates an accuracy limitation. Within this envelope there is an indiscriminate region where sky reflectance signal overlaps with thin foam contribution thus concealing any obvious threshold.

In Fig. 3(c) the total reflectance has a peak at 510 nm but is not as prominent as in the overcast data. This is most likely due to the ship being in a slightly different body of water. In Fig. 3(d) the augmented spectral reflectance profiles are shown for thresholds 4 through 9 (threshold 4 is the mode) . Following similar reasoning as in the overcast case, it seems that the profiles resulting from the application of thresholds 6 and 7 are more realistic. The augmented reflectances are 0.00097 and 0.00085 at 510 nm and 0.00071 and 0.00059 at 860 nm for thresholds 6 and 7 respectively with fractional coverage estimates of 4.8% and 3.4% respectively.

It is interesting to note the relatively higher 440 nm value appearing in the augmented reflectance spectra as it does in the total reflectance profile, whereas in the Fig. 2 data it is relatively low in both the total and augmented reflectance spectra with the application of higher thresholds. This difference is due to measurements taken in slightly different water bodies and to the inclusion of the foam free water color (sky reflection and water-leaving radiance) in measurements of the thinnest foam types and submerged bubbles.

In this example, the augmented reflectance at 670 nm using threshold 6 is marginally highest and the 860 nm has substantially increased in comparison with the overcast example. Also, the augmented reflectance contribution at 670 appears to be consistently higher than at 550 nm, whereas in the overcast example both the 550 and 670 nm values are essentially equal. The augmented reflectance profile suggests a stronger influence from the longer wavelengths. This effect is even more pronounced in the following example.

### **Clear Sky Low Sun**

In Figs. 4(a) - 4(d), data was acquired an hour earlier (at ~7:50 am) on the same day as the data presented in Fig 3. The sun was lower in the sky at approximately 10° above the horizon and at ~80° azimuth from true north. Mean wind speed was 12.1 m/s with a standard deviation of 1.3 m/s during the acquisition period. The wind was out of the north west (325°) and the ship heading was 355°. Air temperature was 12.6°C and water surface temperature 16.55°C (unstable atmosphere). Other parameters from the ship's log were salinity (35.0445 ppt ), barometric

pressure (1019.1 mB) and relative humidity (62%). As in the preceding example, the radiometer was angled  $20^\circ$  away from the direction of the sun to reduce the possibility of sun glitter and specular reflection. The location ( $29.11^\circ$  N,  $84.02^\circ$  W) was approximately 2.7 miles due south of the location where the data in Fig. 4 was taken. During this period of  $\sim 18$  minutes, 7,000 surface reflectance samples were taken. The whitecap development and foam distribution during this acquisition period was similar to the 'clear sky' case, only the sun elevation was smaller.

Figure 4(a) shows the reflectance intervals. In the histogram of the number of samples vs. reflectance levels in Fig. 4(b), the shape of the distribution is similar to that in Fig. 3(b). The distribution rises sharply and falls with a slight broadening towards higher reflectance. The total reflectance shown in Fig. 4(c) is somewhat higher than in Fig. 3(c) data suggesting a possible higher white water contribution. The spectral shape is similar with the exception of relatively higher 410 and 440 nm values. This can be attributed to a spectrally different angular distribution of the downwelling light field. The sky was comprised of a prominently yellow reddish maximum at high zenith angles due to the low sun, and a very rich and dark blue sky toward the zenith - typical of a clear early morning as the sun rises. Horizontal waves and waves inclined away from the low sun reflect the predominantly very blue sky and are most frequently measured by the radiometer. This bias towards more blue measurements accounts for the different shape of the total reflectance profile in this example. However, when plausible threshold reflectance intervals (Fig. 4(d)) are applied in order to estimate the augmented reflectance contribution, the opposite is observed with a bias towards the longer wavelengths.

At threshold interval 5 (mode of the histogram) in Fig. 4(d), the augmented reflectance values at the shorter wavelengths are lower with respect to the longer wavelengths than they were in the total reflectance profile. Using the same criteria from the two previous data sets, white water contribution should begin to appear above the background reflectance in the region of reflectance intervals 6, 7, 8, 9 and maybe 10. Moving up to threshold interval 6, the resulting augmented reflectance spectrum is more accentuated with even lower values towards the blue end and higher values in the red. This is the result of the low sun angle ( $10^\circ$  above the horizon). The augmented

reflectance spectra for threshold 6 yields a 410 nm value (0.00203) that is less than that at 860 nm (0.00265), and with a maximum at 670 nm (0.00313).

Although the spectral shape of the augmented reflectance profiles from thresholds 6, 7 and 8 are somewhat similar, their fractional coverage estimates appear to be too high - 18.5%, 10.9% and 7.9%. Threshold 9 has a more reasonable fractional coverage of 6.0% with an augmented reflectance contribution  $\sim 0.0017$  in the visible. Threshold 10 has a fractional coverage of 4.8% and an augmented reflectance of  $\sim 0.0015$  in the visible. Comparing the fractional coverage and augmented reflectance contribution estimates with the previous example taken under similar conditions (wind speed, air/water temperature, sea state) but with higher sun angle, shows the estimates in this example are much higher; nearly 3 times the augmented reflectance and more than twice the fractional coverage using similar thresholds. These augmented reflectance profiles and their particularly high estimates of fractional coverage suggest that the higher augmented reflectance values at the longer wavelengths may include specular reflections from foam free water facets, although an additional explanation is provided below.

Comparing Figs. 3(d) and 4(d) shows that the augmented reflectance becomes relatively more enhanced in the red and near infrared for the lower solar elevation. Although whitecaps are usually modeled as lambertian reflectors, we believe that this reddening of their reflectance with reduced solar elevation provides indirect evidence of their nonlambertian nature. As the solar elevation is decreased, the contribution to the incident irradiance from the diffuse sky light is enhanced at the expense of the direct sun light. For low solar elevations, the incident irradiance in the blue is almost totally from diffuse sky light. In contrast, the reverse is true in the red, most of the incident irradiance is direct sun light. Let us assume that the whitecaps are lambertian, i.e., they have reflecting properties similar to sheets of white paper floating on the water, and that their reflectance is spectrally neutral throughout the visible. In the red, whitecaps on the side of the waves away from the sun or in the troughs of the waves receive little or no illumination, i.e., they are shadowed from the direct sun. In contrast, in the blue, where the illumination is diffuse, all whitecaps will be illuminated. Thus, in this example, the augmented reflectance would be expected

to *increase* from red to blue because fewer whitecaps are illuminated with red light. In fact, the experimental result [Fig. 4(d)] is exactly the opposite!

Further evidence of the nonlambertian character of whitecaps can be seen by comparing Figs. 3(a) and 4(a). The highest reflectance levels in these figures will be due to the thickest-youngest foam patches. In this case, removal of the ocean background is not relevant to measuring their properties. The reddening of the spectrum in the visible for these foam patches from Figs. 3(a) to 4(a) is very evident. Figure 4(a) shows a strong variation in reflectance with wavelength, a surrogate here for the variation in the angular distribution in of the incident irradiance. In contrast, Fig. 3(a) shows a much more neutral or bluer reflectance for the most-reflective whitecaps. Thus, even for the brightest whitecaps, the dependence of reflectance on the angular distribution of the incident irradiance is clear: they are nonlambertian. However, note that the measurements we have presented here cannot shed light on the actual bi-directional reflection distribution function (BRDF) of the augmented reflectance. The only conclusion we can make regarding the BRDF is that the nadir-viewing augmented reflectance spectrum for diffuse illumination [Fig. 2(d)] and for solar elevations  $>$  about  $30^\circ$  are similar.

The nonlambertian nature of whitecaps and its relationship to the solar elevation is easy to understand. Whitecaps are isolated volume scatterers, and at low solar elevations the solar beam can enter the sides as well as the top of the whitecap and be scattered out toward the zenith. In contrast, for high elevations or for diffuse illumination relatively fewer photons will enter the sides, and this results in a lower overall reflectance.

## **Open Ocean Data**

The data used here were acquired from a transect of the Pacific Ocean from Manzanillo, Mexico ( $19.03^\circ$  N,  $104.20^\circ$  W) to Honolulu, Hawaii ( $21.20^\circ$  N,  $157.55^\circ$  W). Only data which were acquired under relatively constant and overcast conditions were used to model augmented reflectance with other parameters such as wind speed etc. These data sets have a well behaved

background in terms of radiometrically determining a threshold between white water and nonwhite water events. Overcast conditions also provide a better downwelling light description for correction of the deck cell cosine collector [Moore *et al.*, 1997]. Other whitecap data were acquired during broken sky and scattered cloud conditions, but have not been included in the modeling. The threshold is more difficult to define for these data sets, due to the large variability and random nature of the downwelling light field and its effect on surface reflectance measurements.

The data used are from 4 different days and locations during the transect. Wind speed was relatively constant and remained within a range of 1-2 m/s for days at a time. Reflectance data was acquired for wind speeds between ~8 - 13 m/s. Stability of the lower atmosphere, defined by the air temperature / water temperature differential, varied from neutral to slightly unstable. Other parameters such as salinity, humidity and barometric pressure were also recorded for possible correlation.

The reflectance interval resolution was increased from the previous value of 0.0025 to 0.001. While more threshold choices were generated as result of the higher resolution, it was primarily implemented to monitor background stability by observing the distribution of reflectance intervals verses number of samples. In cases where the sun came out from behind the clouds or a cloud blocked the sun, the foam free water surface reflectance either decreased or increased. This was observed as a broadening (sometimes with bumps) in the distribution of reflectance interval vs. number of samples for given data set.

In Fig. 5 the augmented reflectance contribution from 17 data sets is presented as a function of wind speed. Each of the 17 augmented reflectance data points were acquired from an average acquisition time of 45 minutes (or ~800 m<sup>2</sup> surface area). For clarity, the augmented reflectances from wavebands 410 nm through 550 nm (ARC<sub>410-550</sub>) have been averaged since their values vary only slightly with respect to one another. The augmented reflectance at 670 nm (ARC<sub>670</sub>) which also varies only slightly with the other visible wavebands, and the augmented spectral reflectance at 860 nm (ARC<sub>860</sub>) which is always distinctly lower than the visible wavebands are shown. To relate augmented reflectance to wind speed a power law relationship has been applied in the same

vein as previous authors have related fractional coverage to wind speed [*Blanchard, 1971; Ross and Cardone, 1974; Wu, 1979; Toba and Chaen, 1973; Monahan and O'Muircheartaigh, 1980,1986*]. For a given wind speed the augmented reflectance contribution in the 410-550 nm region can be related to the wind speed with a correlation of 0.702 by:

$$ARC_{410-550} = 9.648 \times 10^{-7} U^{2.777}$$

where  $ARC_{410-550}$  is the augmented reflectance contribution as described above and  $U$  is the wind speed in meters per second. Thus, the wind speed accounts for about half of the variance in  $ARC_{410-550}$ . For the augmented reflectance contribution at 670 nm and 860 nm we have:

$$ARC_{670} = 1.131 \times 10^{-6} U^{2.698}$$

and

$$ARC_{860} = 1.302 \times 10^{-6} U^{2.545}$$

with correlation factors of 0.699 and 0.647, respectively. Data taken during scattered and partly cloudy conditions, although not used in determining the above relationship, are also shown in Fig. 5. These data were acquired with sun elevation greater than 50°. Reducing this data was more complex due to a variable threshold but the results are similar to the data acquired under steady overcast conditions with a well defined threshold.

In Fig. 6 the respective fractional coverage estimates are plotted as a function of wind speed. The distribution of fractional coverage estimates for a given wind speed appear to be more scattered than for augmented reflectance.

In Fig. 7 the relationship between augmented reflectance contribution ( $ARC_{410-550}$ ) and fractional coverage can be expressed as a linear relationship with a correlation of 0.694 given by:

$$\text{ARC}_{410-550} = 9.252 \times 10^{-3} W + 0.000195$$

where  $W$  is the fractional coverage.

A scatter plot of the percentage drop in augmented reflectance from  $\text{ARC}_{410-550}$  to  $\text{ARC}_{860}$  is shown in Fig. 8. A linear fit is applied between the data points to indicate an increasing trend in the drop off between  $\text{ARC}_{410-550}$  and  $\text{ARC}_{860}$  with wind speed rather than to establish a model, as the correlation is very low, 0.359. However, the data indicate that for wind speeds in the range 8-12 m/s the percentage drop off between  $\text{ARC}_{410-550}$  and  $\text{ARC}_{860}$  is approximately 15 - 25%.

Possible correlations between the augmented reflectance and other parameters such as water temperature, air temperature, stability of the lower atmosphere, humidity, salinity, barometric pressure, wave height, sea swell were investigated. No correlations could be established mainly due to the small variation in the parameters during the transect.

## Discussion

In this paper we have shown examples of whitecap spectra of different foam types and reflectances, both from individual whitecaps and as an integrated sum over a period of time expressed as the augmented reflectance contribution and fractional coverage. From the first cruise, estimates of the augmented spectral reflectance contribution and fractional coverage have been obtained from measurements taken under different sky conditions and sea states but with similar wind speeds in order to highlight the variability of whitecap formation and the difficulties in providing accurate information on the optical influence of whitecaps. From the second cruise, estimates of augmented spectral reflectance and fractional coverage acquired during overcast skies and more consistent weather conditions with essentially unlimited fetch and duration have been derived for ocean color satellite waveband correction and atmospheric correction algorithms.

Of particular importance is the determination of the threshold required to accurately determine augmented spectral reflectance contribution and fractional coverage. Despite the application of high

resolution white water threshold reflectance intervals, the threshold choice remains difficult and somewhat subjective. Regardless of the threshold resolution that may be applied, the very wave nature of the water surface and the distribution of the downwelling light field creates an inseparable and indiscriminate region between foam and foam free contributions. As mentioned earlier, the reflectance of foam in the shadow of an adjacent wave may result in a lower reflectance than a foam free water facet reflecting a bright region of the sky. Choice of threshold is further compounded since the thinnest foam types, which are close to the threshold reflectance, are very important due to their long endurance. Without adequate discrimination of the thinner foam type, the estimation of fractional coverage and augmented spectral reflectance contribution will always incur some error. Utilization of a higher threshold resolution and the subsequent inclusion of the less reflecting and thinnest foam types results in fractional coverage estimates that are roughly 3 times higher than that reported by other researchers [*Blanchard, 1971; Ross and Cardone, 1974; Wu, 1979; Toba and Chaen, 1973; Monahan and O'Muircheartaigh, 1980,1986*]. The ratio of the augmented reflectance contributions in the visible to the fractional coverage estimates determined with this system results in an effective reflectance of  $\sim 1.25\%$ . This much lower effective reflectance than the 22% determined by *Koepke [1984]* gives an indication of the greater quantity of thin foam and foam streaks that have been included in these measurements.

From the data used in this paper, the fractional coverage has been observed to vary by a larger amount than the augmented reflectance contribution in going from one threshold interval choice to another. This is due to the definition of fractional coverage which is not weighted by reflectance, and as result, the thinnest foam patches are assumed equal in reflectance to the more highly reflecting thick, dense foam types. The augmented spectral reflectance contribution is the more meaningful measurement for satellite observations whereas fractional coverage must be combined with reflectance data to achieve the same result.

Examples from the first cruise in the Gulf of Mexico reveal the dependence of whitecap formation on parameters other than the wind speed measured at the time of observation. The examples described from the first cruise all had similar wind speeds. Changing weather conditions

such as during the onset of a cold front produced higher values of augmented reflectance and fractional coverage ('overcast') than when conditions had been consistent for a longer period of time ('clear sky', 'clear sky low sun'). For the 'overcast' example, the lower atmosphere was essentially neutral ( $\Delta T = T_{\text{air}} - T_{\text{water}} = -0.8^{\circ}\text{C}$ ) and produced high augmented reflectance and fractional coverage estimates. By the next day, the sea state under the influence of conditions of greater duration produced augmented reflectance and fractional coverage estimates that were roughly 1/3 those obtained during the onset of the cold front, despite the atmosphere being unstable (i.e.  $\Delta T = T_{\text{air}} - T_{\text{water}} = \sim -4^{\circ}\text{C}$ ). The whitecaps visually appeared different to those in the 'overcast' case with large breaking waves, although less frequent, and with more residual foam patches and foam streaks that were essentially absent in the 'overcast' case. Nevertheless, one would expect the opposite result with greater whitecap influence during unstable atmospheric conditions and less during neutral conditions. On the other hand, the augmented reflectance and fractional coverage for the 'clear sky low sun', which had similar whitecap and foam conditions to the 'clear sky' case, produced values roughly twice the 'clear sky' values due to the effects of the low sun. The dependence on sea state, wind variations with rising or falling trend, change in wind direction, minimal fetch and duration along with specular sun reflections, whitecap BRDF effects, and low sun angles are responsible for these differences in fractional coverage and augmented spectral reflectance for similar wind speeds. The data from the Gulf of Mexico was taken roughly 110 km offshore which is an adequate fetch for 12 m/s wind speeds [Ross and Cardone, 1974]. The estimate of the augmented reflectance from the 'clear sky' case, which was acquired under sea state conditions with adequate fetch and duration, and under illumination conditions that were not particularly extreme (sun elevation of  $30^{\circ}$ ), produced similar results to the open ocean data taken in the Pacific.

Another interesting aspect resulting from these examples is the spectral change in the upwelling signal during low sun angle. The spectral variation in estimates of the augmented reflectance contribution seems to be dependent on sea state and the whitecap morphology. In Fig. 2(d) the decrease from the 440 nm to the 860 nm value is  $\sim 41\%$  from observation of many small

whitecaps and very few residual and fragmented foam patches. From Fig. 3(d) the drop in augmented reflectance from 440 nm to 860 nm is ~28% from observation of a few large whitecaps but mostly residual and patchy foam. We attribute the significant change in the spectral variation of whitecap reflectance from the 'clear sky' to the 'clear sky low sun' examples to the nonlambertian nature of the whitecaps (the BRDF effect). This effect could also influence the magnitude the drop from 440 to 860 nm.

Since the low sun has this influence on the augmented reflectance (and fractional coverage), the wind direction with respect to the sun becomes an important consideration. The longitudinal axis of waves (and whitecaps) are more or less perpendicular to the direction of the wind. In the 'clear sky low sun' case, the wind is from the north-west at 325° with the sun at 80° azimuth with respect to true north. This results in whitecaps and the crests of waves being illuminated at ~25° incident angle (azimuth). One might expect a maximum effect if the wind had been from the west at 260° or perhaps from the east at 80° azimuth and a minimal effect with the wind from the north at 350° or south at 170° azimuth.

The goal of this study is to determine the augmented reflectance contribution from whitecaps as viewed from satellites and, in particular, its spectral dependence. Useful satellite data of the ocean is taken around solar noon and from cloud free regions. The low sun angle examples (10° and 30° above the horizon) used here can be considered extreme conditions and are not frequently encountered. However, it brings attention the effect low sun angle has on the augmented reflectance contribution. This effect may have particular importance for higher latitude waters both north and south of the equator where, during the winter months or even in higher latitudes in the summer months, the sun maintains a low angle above the horizon at around midday. For higher sun elevation, the BRDF effect (although substantially reduced) may still exist. These high latitude waters are particularly prolific as regards phytoplankton blooms, triggered by seasonal nutrient rich cold upwellings. They are often windy areas with an abundance of whitecaps and a bias of the reflectance towards the yellow-red end of the visible spectrum. with low sun angle, brings attention to the 670 nm waveband near the phytoplankton fluorescence peak at 685 nm. The

Moderate Resolution Imaging Spectroradiometer (MODIS) sensor [Salmonson, 1989] will be capable of estimating this phytoplankton fluorescence signal [Letelier and Abbott, 1996]. This fact adds to the importance whitecaps may play in these higher latitudes. And of course, the high values at 670 and 860 nm at lower sun angles, from a combination of whitecaps and foam free waves, could complicate atmospheric correction algorithms unless adequately characterized.

The spectral characteristics of the augmented reflectance found in both the Gulf of Mexico and from the Pacific Ocean seem to possess some spectral characteristics that are related to the water color properties in which they were formed. In Fig. 9 examples of the nonwhite water spectral profiles and their augmented reflectances from both water bodies are shown. Both examples were taken under overcast sky conditions. For Gulf of Mexico waters, the augmented reflectance from threshold interval 20 in the 'overcast' case is used and the augmented reflectance and the nonwhite water spectrum have distinctly lower 410 nm values than their respective 440 nm values. For the very blue and clear Pacific Ocean waters, the 410 nm value is higher than the 440 nm value in both the augmented reflectance and nonwhite water spectral profiles.

The augmented reflectance profile in Fig. 9 for the Pacific Ocean has been compiled by averaging the normalized augmented reflectance of each of the 17 data samples used in earlier modeling. The difference between each channel of the mean augmented reflectance profile shown and the mean  $ARC_{410-550}$  is +2.9%, -6.0%, +6.1%, -3.1%, -2.4% and -21.6%. The standard deviation for each waveband over the 17 data points is typically less than, or about equal to, the size of the symbols in Fig. 9. For the augmented reflectance from the Gulf of Mexico the difference between each channel and its  $ARC_{410-550}$  is -4.5%, -1.8%, +7.0%, -0.8%, -2.1% and -42.2%.

In both cases, the augmented reflectances are similar with the exception of the 410 and 860 nm values. The 860 nm value is lower in the Gulf of Mexico example due to a different type of wave breaking (many small whitecaps suddenly appeared at the onset of a cold front yielding very high augmented reflectance and fractional coverage estimates). Although the 410 nm value of the augmented reflectance seems to be related to the water in which it was formed, the 510 nm value

does not and would appear to be independent of water color type. A similarly low 410 nm value was observed in foam data generated by a ship's wake in coastal waters off the coast of Southern California [Moore *et al.*, 1997]. The low 410 nm value may be influenced by the higher absorption properties of coastal waters at the shorter wavelengths, but the enhanced absorption alone cannot explain this effect. Initially it was thought that this coupling between the augmented reflectance and the water type in which the white water is formed might be explained by the inclusion of very thin foam types where a good proportion of the background water color is also measured. But this does not explain the apparent indifference of wavebands above 410 nm (and perhaps 440 nm) to the foam free background water color.

Although most of our open ocean analysis utilized only data acquired during overcast conditions (to facilitate more accurate estimation of the background water reflectance threshold, and to eliminate sun glint, which is easy to mistake for thin foam), some data for partly cloudy and clear skies were examined. This partly cloudy/clear sky data possessed an augmented reflectance spectrum similar to the overcast cases, as well as similar values of  $ARC_{410-550}$  (Fig. 5). Thus, we believe that our ARC results should be reasonably representative of clear sky situations, and thus useful for estimating the whitecap contribution to the reflectance measured by ocean color sensors.

## Conclusions

To summarize, spectral characteristics found in the augmented reflectance can be influenced by a number of factors such as sky condition (e.g. bright horizon and overcast sky), solar elevation, sea state; type of wave breaking and direction of wave breaking (particularly at low solar elevation). The spectral profile of the augmented reflectance contribution may even be dependent on the color properties of the water body in which the whitecap forms, since the detection of very thin foam types include upwelling water-leaving radiance contributions. Despite the inaccuracies in determining the white water threshold, the spectral profile of the augmented reflectance remains consistent over a large number of reasonable threshold choices. Threshold determination is inherently complicated and subject to some error due to the overlap of white water and nonwhite

water reflectance contributions. For most applications, any subtle spectral characteristics found in the estimates of the augmented reflectance, besides the distinctive lower 860 nm value, are overshadowed by the inaccuracy in determining the correct white water to nonwhite water threshold.

We have determined the augmented reflectance contribution in the open ocean for the 410 - 550 nm range to be 0.00031 at a wind speed of 8 m/s, 0.00058 at 10 m/s and 0.00096 at 12 m/s with a standard deviation of 0.000108. These results are somewhat lower than previously derived values of whitecap optical influence [Koepke, 1984; Gordon and Wang, 1994b]. Using Koepke's effective reflectance of 22% and the fractional coverage determined by wind speed for water temperature above 14°C [Monahan and O'Muircheartaigh, 1980] yields values that are greater than 4 times our values at 12 m/s and roughly 3 times at 8 m/s. Applying the fractional coverage relationship which takes into account atmospheric stability [Monahan and O'Muircheartaigh, 1986], our results are still lower even when assuming a very stable atmosphere. Also the 860 nm value, which may be an indicator of the type of wave breaking responsible for the amount and depth of bubbles forced into the water column, is found to be 15%-20% lower than the optical influence of whitecaps in the visible for wind speeds 8 - 12 m/s in the open ocean, i.e., half of that observed by Frouin *et al.* [1996] in the surf zone. We have ascertained the augmented reflectance contribution at 860 to be 0.00026 at wind speed of 8 m/s, 0.00046 at 10 m/s and 0.00073 at 12 m/s. This implies a lower contribution from whitecaps at 860 nm (~5.6 times lower for wind speeds at 12 m/s and ~3.8 times lower for wind speeds of 8 m/s using the Koepke [1984] effective reflectance of 22% and the Monahan and O'Muircheartaigh [1980] wind speed to fractional coverage relationship).

Koepke [1984] concluded that the optical influence of oceanic whitecaps was in fact less important than had been previously assumed since his effective reflectance reduced the optical influence of whitecaps by a factor of 2. Certainly from our direct measurements of the optical influence of whitecaps and foam in the 8 - 12 m/s wind speed range suggest that whitecap optical influence can be considered to be even less important than Koepke's optimistic conclusion.

## Notation

|                 |  |
|-----------------|--|
| $ARC_{410-550}$ | mean augmented reflectance contribution from values at 410, 440, 510 and 550 nm. |
| $ARC_{670}$     | augmented reflectance contribution at 670 nm.                                    |
| $ARC_{860}$     | augmented reflectance contribution at 860 nm.                                    |
| $T_{air}$       | air temperature  |
| $T_{water}$     | water surface temperature  |
| $\Delta T$      | temperature differential ( $\Delta T = T_{air} - T_{water}$ );                   |
| $U$             | wind speed in meters per second  |
| $W$             | fractional coverage of whitecaps and foam  |

**Acknowledgments.** This research was funded by NASA / EOS - MODIS, Goddard Space Flight Center under contract #NAS5-31363. We would like to thank Al Chapin for his help in the design and construction of the equipment. Also our thanks to Dr. Rik Wanninkhof (NOAA/AOML) and Dr. Gary Hitchcock (RSMAS/University of Miami) for allowing us to participate in their oceanographic excursion on the R/V Malcolm Baldrige in the Gulf of Mexico. We would like to thank the NOAA personnel: CMDR Mark Koehn, LCDR Tim Wright (TAO Operations Manager) and Lt. John Herring for allowing us to join their transit of the Pacific Ocean aboard the R/V Ka'imimoana.

## References

Blanchard, D. C., Whitecaps at sea. *J. Atmos. Sci.*, 28, 645, 1971.

Bortkovskii, R. S., and V. A. Novak, Statistical dependencies of sea state characteristics on water temperature and wind-wave age. *J. of Marine Systems*, 4, 161-169, 1993.

Cardone, V. J., Specification of the wind field distribution in the marine boundary layer for wave forecasting. *Rep. TR 69-1*, Geophys. Sci. Lab., New York Univ., New York, December 1969.

Frouin, R., M. Schwindling and P. Y. Deschamps, Spectral Reflectance of Sea Foam in the Visible and Near Infrared: In Situ Measurements and Remote Sensing Implications. *J. Geophys. Res.*, 101C, 14361-14371, 1996.

Garrett, W. D., The influence of surface-active material on the properties of air bubbles at the air/sea interface. *Rep. Naval Research Lab.*, 6545, Washington D.C., 14 pp., 1967.

Gordon, H. R., and M. M. Jacobs, Albedo of the Ocean-Atmosphere System: Influence of Sea Foam. *Applied Optics*, 16, 2257-2260, 1977.

Gordon, H. R., and M. Wang, Retrieval of water-leaving radiance and aerosol optical thickness over the oceans with SeaWiFS: A preliminary algorithm, *Applied Optics*, 33, 443-452, 1994a.

Gordon, H. R., and M. Wang, Influence of oceanic whitecaps on atmospheric correction of SeaWiFS, *Applied Optics*, 33, 7754-7763, 1994b.

Koepke, P., Effective Reflectance of Oceanic Whitecaps. *Applied Optics*, 23, 1816-1824, 1984

Letelier, R. M., and M. R. Abbott, An analysis of chlorophyll fluorescence algorithm for the moderate resolution imaging spectroradiometer (MODIS), *Remote Sensing Environment*, 58, 215-223, 1996.

Maul, G. A., and H. R. Gordon, On the Use of Earth Resources Technology Satellite (LANDSAT-1) in Optical Oceanography. *Remote Sensing Environment*, 4, 95, 1975.

Miyake, Y., and T. Abe, A study on the foaming of sea water. *J. Marine Res.*, 7, 67-73, 1948.

Monahan, E. C., and C. R. Zietlow, Laboratory comparisons of fresh-water and salt-water whitecaps. *J. Geophys. Res.*, 74, 6961-6966, 1969.

Monahan, E. C., Oceanic whitecaps. *J. Physical Oceanogr.*, 1, 139-144, 1971.

Monahan, E. C., and I. G. O'Muircheartaigh, Optimal power-law description of oceanic whitecap coverage dependence on wind speed. *J. Phys. Oceanogr.*, 10, 2094-2099, 1980.

Monahan, E. C., and I. G. O'Muircheartaigh, Whitecaps and passive remote sensing of the ocean surface. *Int. J. Remote Sens.*, 7, 627-642, 1986.

Moore, K. D., Voss, K. J., Gordon, H. R., 1997: Spectral reflectance of whitecaps: Instrumentation, calibration and performance in coastal waters. Submitted *J. Atmospheric and Oceanic Technology*. December 1996.

- Payne, R. E., Albedo of the Sea Surface. *J. Atmospheric Physics*, 29, 959-970, 1972.
- Ross, D. B., and V. J. Cardone, Observations of oceanic whitecaps and their relation to remote measurements of surface wind speed. *J. Geophys. Res.*, 79, 444-452, 1974.
- Salmonson, V. V., W. L. Barnes, P. W. Maymon, E. H. Montgomery and H. Ostrow, MODIS: Advanced facility instrument for studies of the earth as a system, *IEEE Geosci. Rem. Sens.*, 27, 145-152, 1989.
- Toba, Y., and M. Chaen, Quantitative expression of the breaking of wind waves on the sea surface. *Rec. Oceanogr. Works*, 12, 1-11, 1973.
- Whitlock, C. H., D. S. Bartlett, and E. A. Gurganus, Sea foam reflectance and influence on optimum wavelength for remote sensing of ocean aerosols. *Geophys. Res. Letters*, 9, 719-722, 1982.
- Wu, J., Oceanic whitecaps and sea state. *J. Phys. Oceanogr.*, 9, 1064-1068, 1979.
- Wu, J., Variation of whitecap coverage with wind stress and water temperature. *J. Phys. Oceanogr.*, 18, 1448-1453, 1988.

## Figure Captions

Fig. 1(a). Time series of the reflectance of two whitecaps and their foam types passing in view of the radiometer.

Fig. 1(b). Reflectance spectra of the two whitecaps of Fig. 1(a) reduced to reflectance intervals.

Fig. 2(a). Reflectance spectra of ~9,000 water surface reflectance samples from 'overcast' data reduced to reflectance intervals.

Fig. 2(b). Histogram of the number of reflectance samples per reflectance interval for 'overcast' data.

Fig. 2(c). Total reflectance of 'overcast' data (the sum of all weighted reflectance intervals). This is equivalent to the upwelling signal detected by a satellite assuming no atmospheric contribution.

Fig. 2(d). Augmented spectral reflectance contribution for a range of reflectance interval threshold choices. The fractional coverage estimate for each augmented reflectance profile is shown. For higher threshold choices the contributions in the visible region equalize with the exception of the 410 nm and 860 nm contributions.

Fig. 3(a). Reflectance spectra of ~10,000 water surface reflectance samples from 'clear sky' data (sun elevation of ~30° above horizon) reduced to reflectance intervals.

Fig. 3(b). Histogram of the number of reflectance samples per reflectance interval for 'clear sky' data.

Fig. 3(c). Total reflectance of 'clear sky' data (the sum of all weighted reflectance intervals). This is equivalent to the upwelling signal detected by a satellite assuming no atmospheric contribution.

Fig. 3(d). Augmented spectral reflectance contribution for a range of reflectance interval threshold choices. The fractional coverage estimate for each augmented reflectance profile is shown. Note the higher 670 nm and 860 nm values due to the influence of the longer wavelengths from a low sun.

Fig. 4(a). Reflectance spectra of ~7,000 water surface reflectance samples from 'clear sky low sun' data (sun elevation of ~10° above horizon) reduced to reflectance intervals.

Fig. 4(b). Histogram of the number of reflectance samples per reflectance interval for 'clear sky low sun' data.

Fig. 4(c). Total reflectance of 'clear sky low sun' data (the sum of all weighted reflectance intervals). This is equivalent to the upwelling signal detected by a satellite assuming no atmospheric contribution.

Fig. 4(d). Augmented spectral reflectance contribution for a range of reflectance interval threshold choices. The fractional coverage estimate for each augmented reflectance profile is shown. Note the much higher 670 nm and 860 nm and lower 410 nm values due to the influence of the longer wavelengths from a low sun. The 410 nm value is lower than the 860 nm value for all threshold choices.

Fig. 5. Augmented reflectance contribution for different wind speeds from open ocean data taken in the equatorial Pacific. Data points of the augmented reflectance from different waveband regions and their power law relationships with wind speed are shown.  $ARC_{410-550}$  is the mean

augmented reflectance of wavebands 410, 440, 510 and 550 nm.  $ARC_{670}$  and  $ARC_{860}$  are the augmented reflectance for the 670 and 860 nm wavebands respectively.  $ARC_{410-550} PC /$  scattered is for data taken under partly cloudy and scattered conditions (solar elevations  $\sim 50^\circ$ ) and not used in establishing power law relationship.

Fig. 6. Fractional coverage vs. wind speed for same data used in Fig. 5. A power law relationship is applied although the fractional coverage values are more varied for a given wind speed.

Fig. 7. Fractional coverage vs. mean augmented reflectance of 410, 440, 510 and 550 nm values. A linear fit is applied with a reasonable correlation of 0.694. Wind speed is shown for each data point.

Fig. 8. Percentage drop in the augmented reflectance between  $ARC_{410-550}$  and  $ARC_{860}$  for wind speeds in the 8 - 12 m/s range. The linear fit indicates an increasing trend with higher wind speed.

Fig. 9. Augmented and nonwhite water reflectance profiles normalized at 510 nm (not to scale) are shown for data taken in the Pacific Ocean and the Gulf of Mexico. The augmented reflectance for the Pacific Ocean is compiled from all data presented in this paper used to estimate the optical influence of whitecaps. Note the similarities in augmented reflectance profiles regardless of the water color in which the whitecaps form. The 410 nm value seems to be the exception and mimics the nonwhite water reflectance in both cases. The 860 nm value, which may be used to indicate the type of wave breaking, is lower in the Gulf of Mexico data due to type of whitecaps formed by the sudden arrival of a cold front.

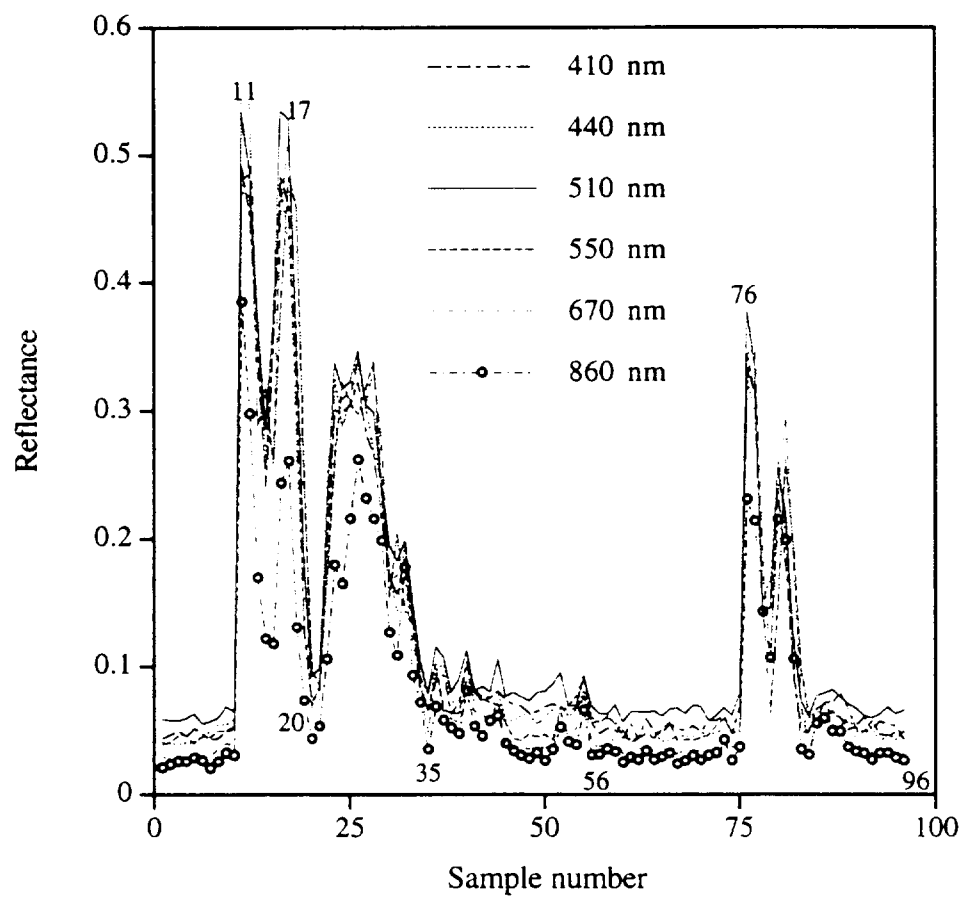


Fig. 1(a)

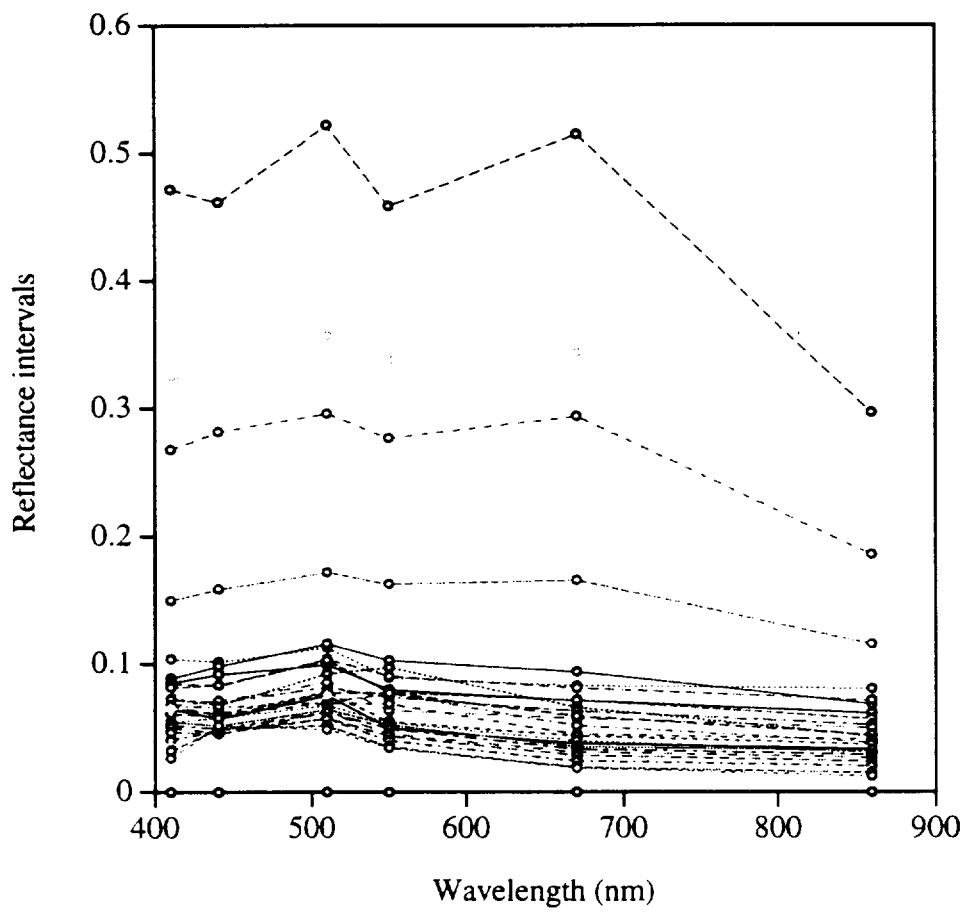


Fig. 1(b)

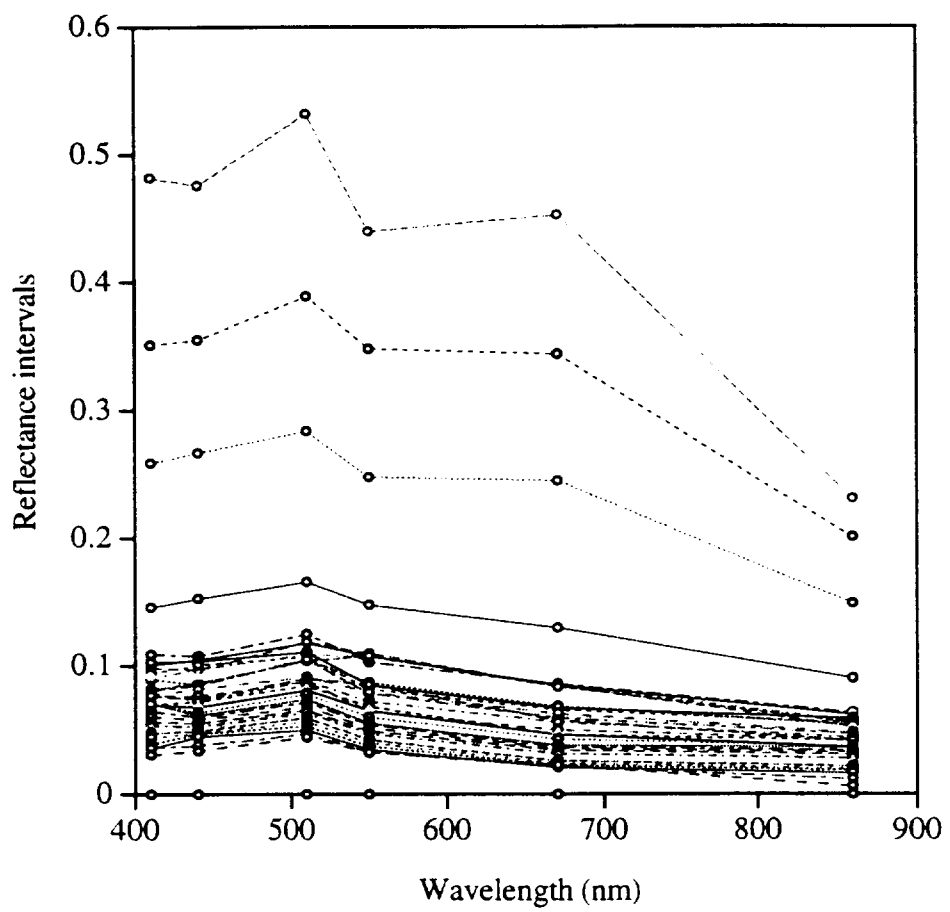


Fig. 2(a)

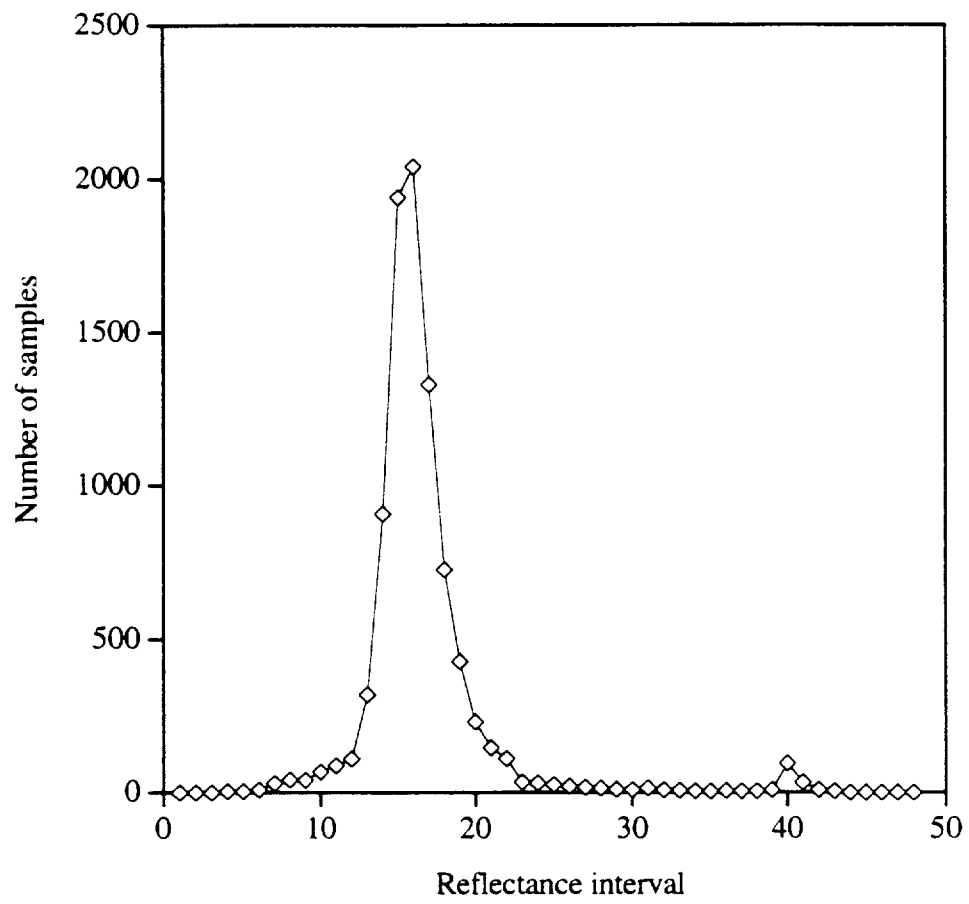


Fig.2(b)

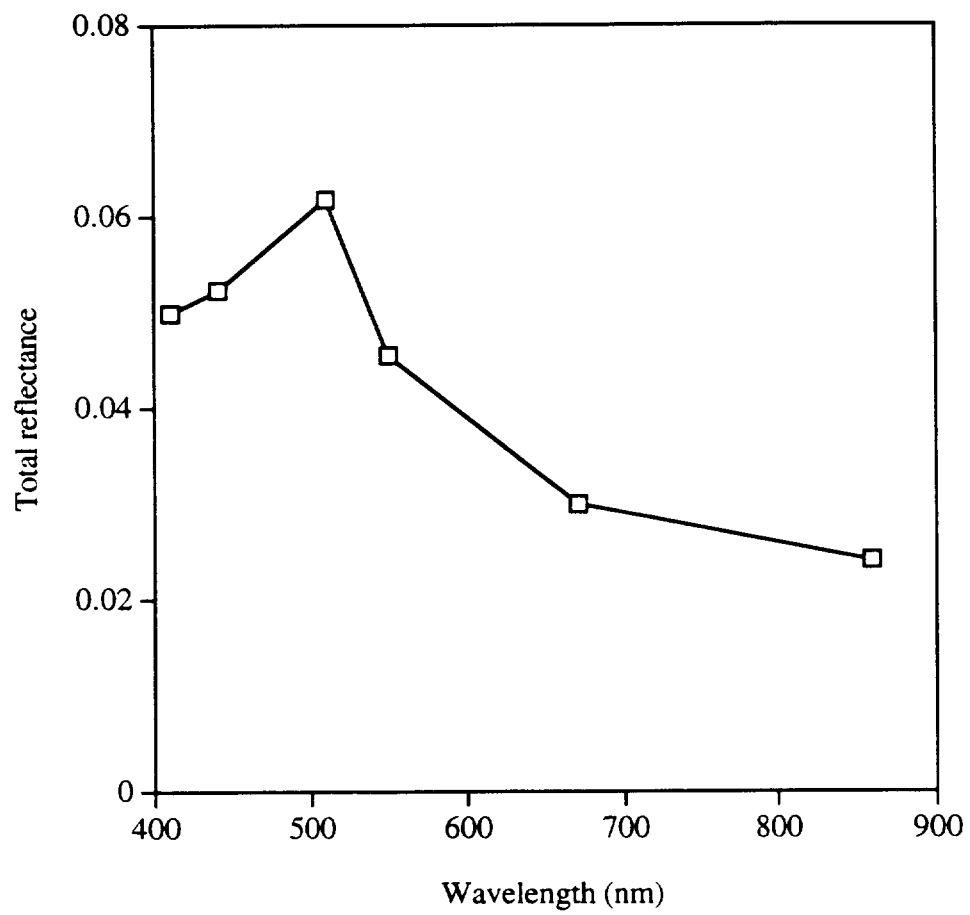


Fig. 2(c)

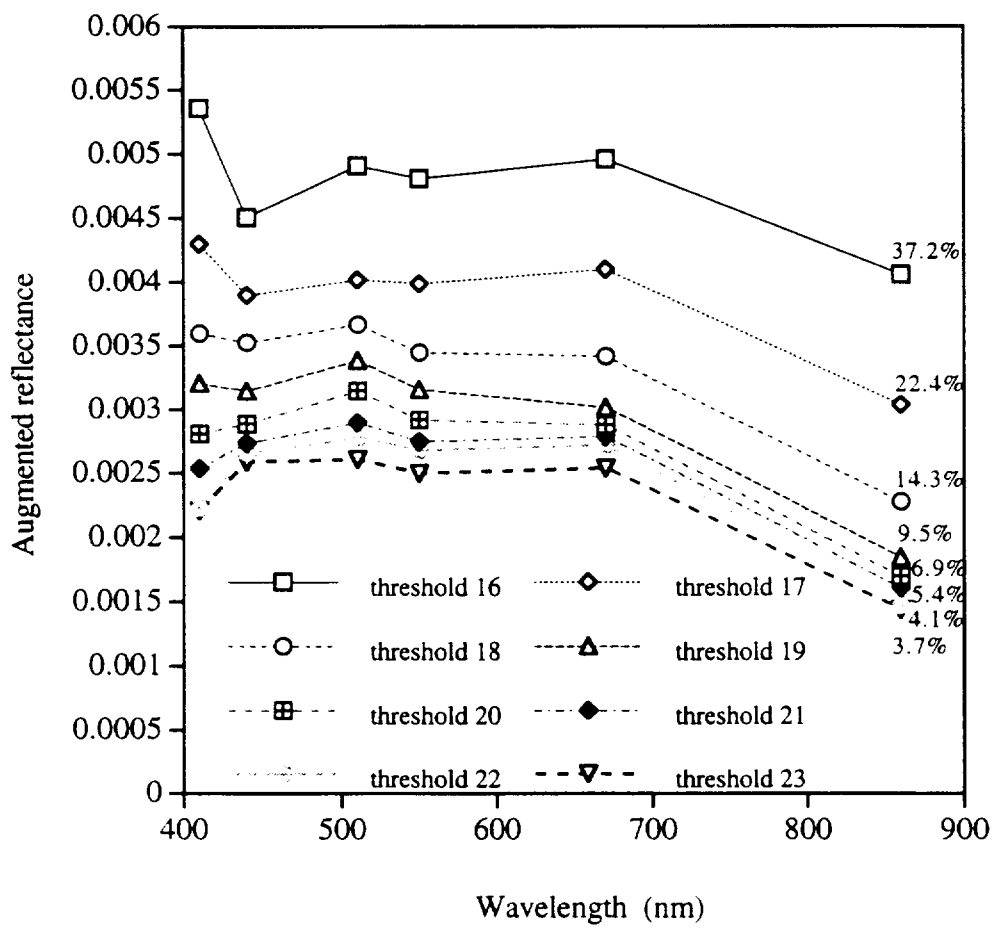


Fig. 2(d)

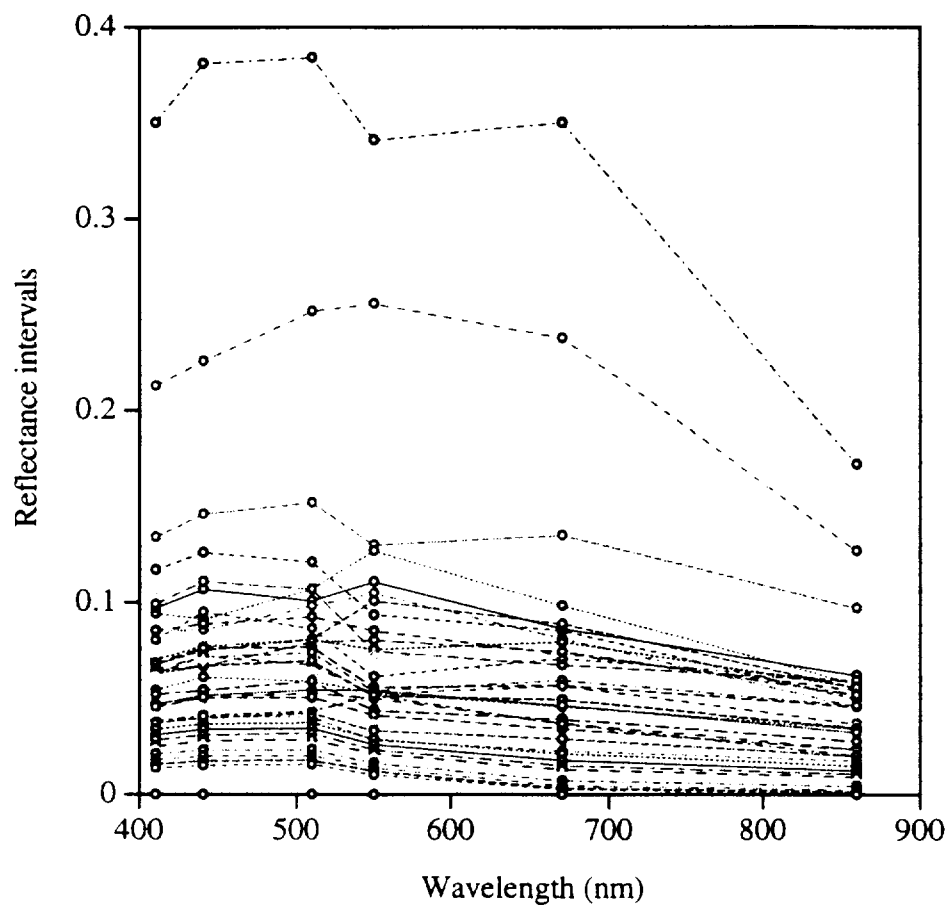


Fig. 3(a)

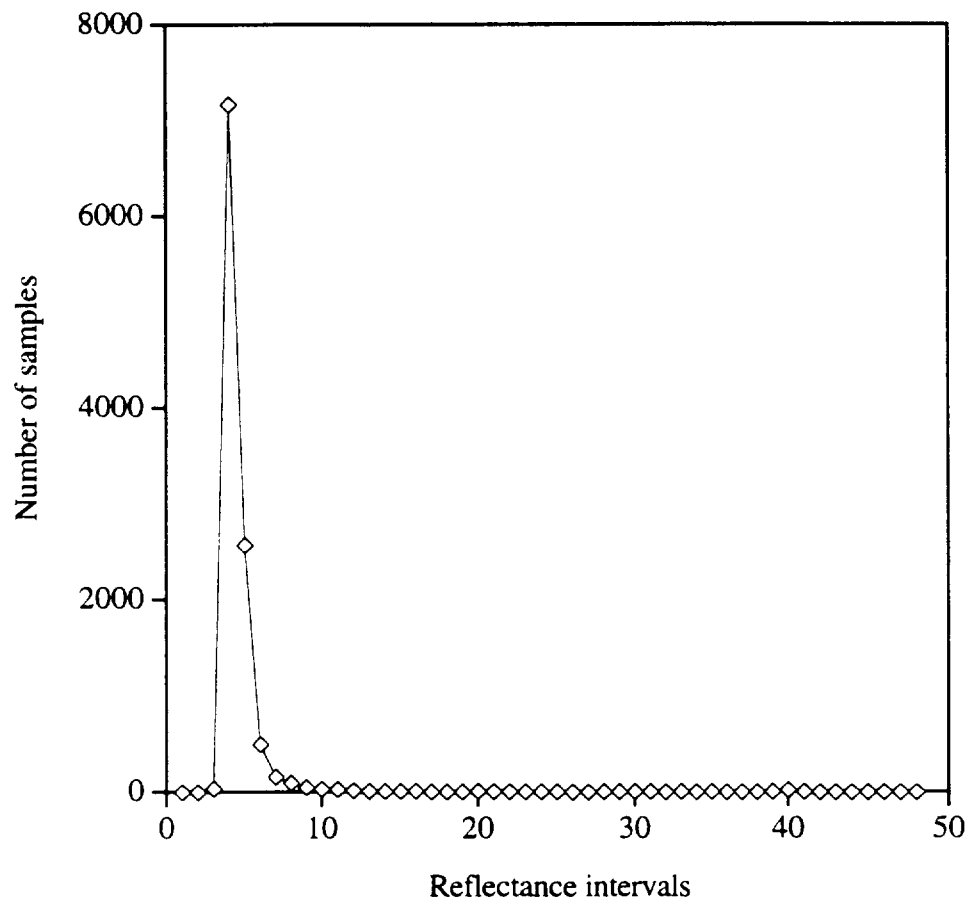


Fig. 3(b)

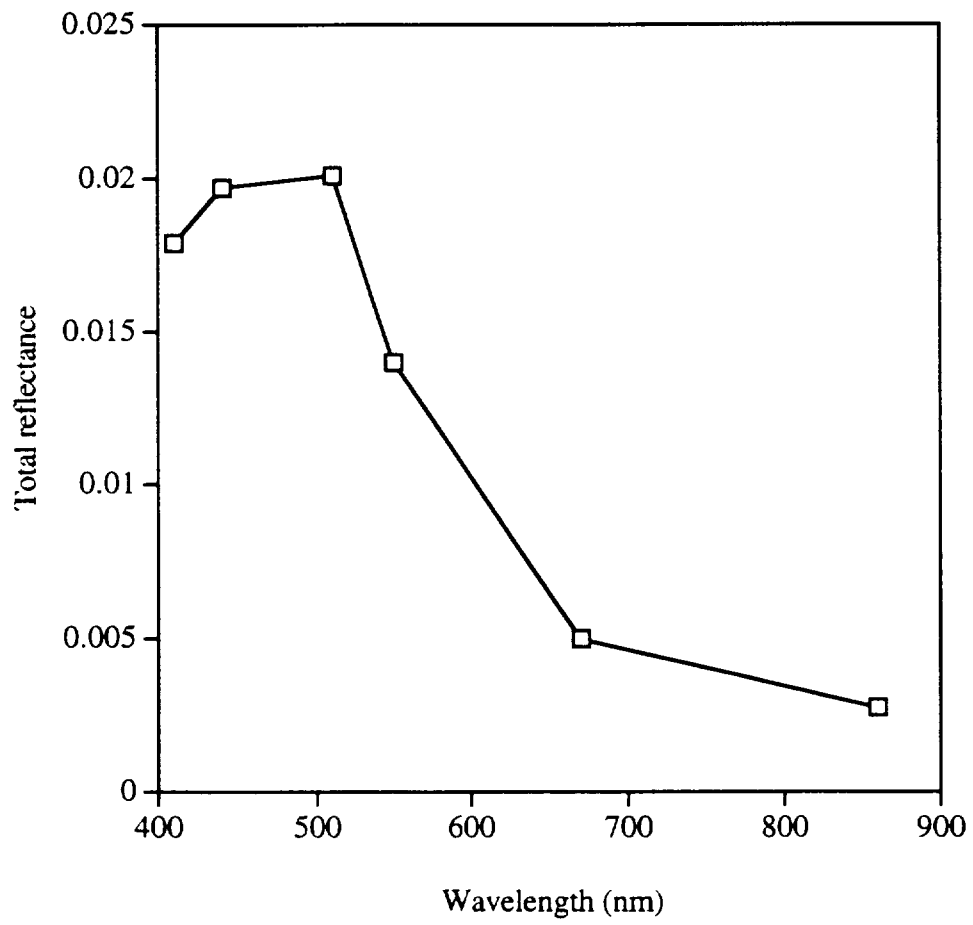


Fig. 3(c).

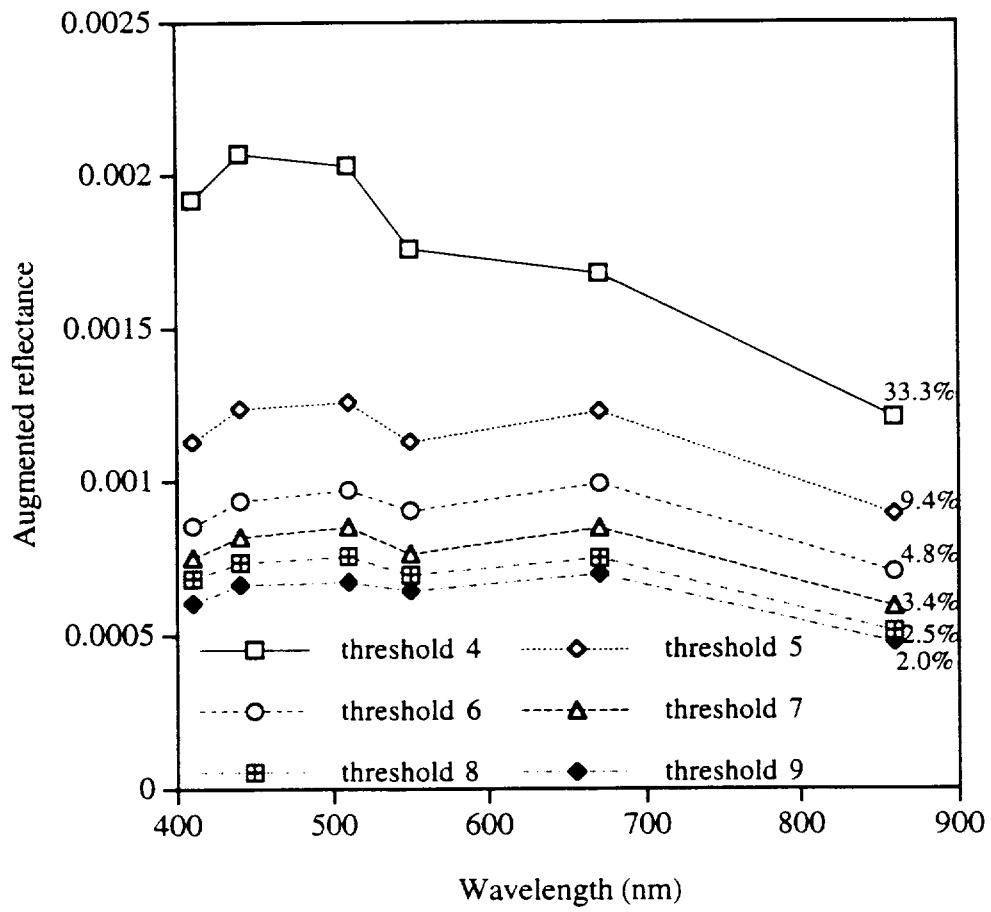


Fig. 3(d).

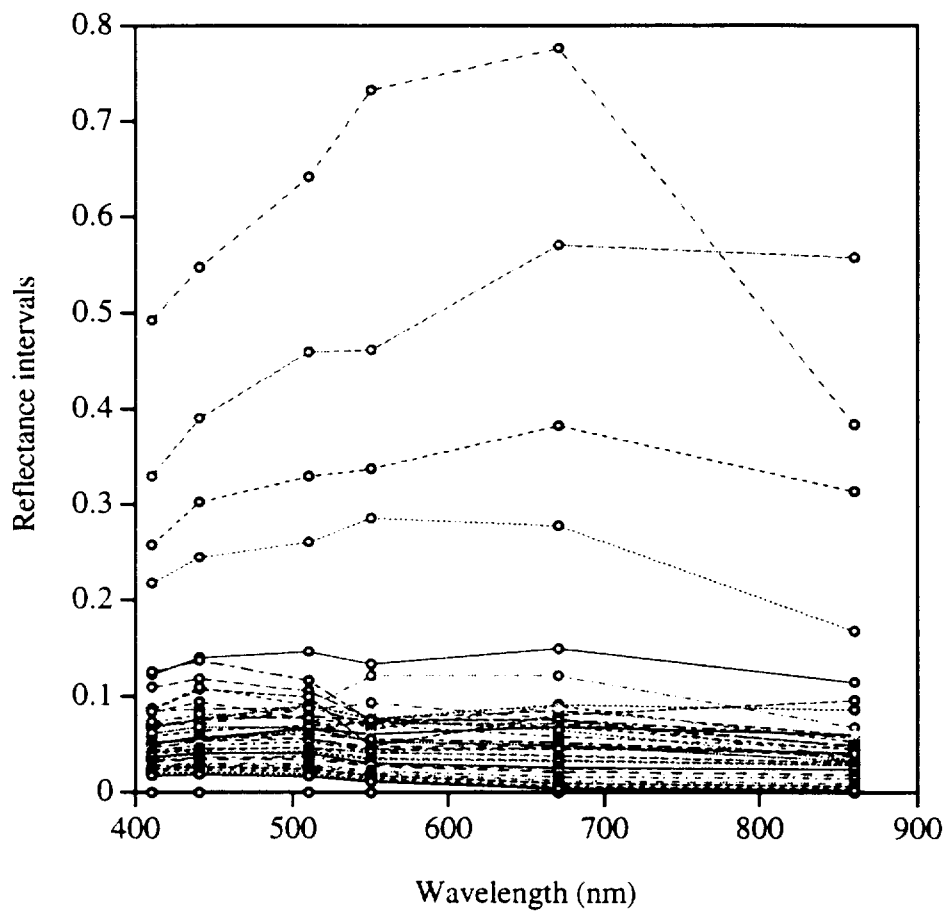


Fig. 4(a).

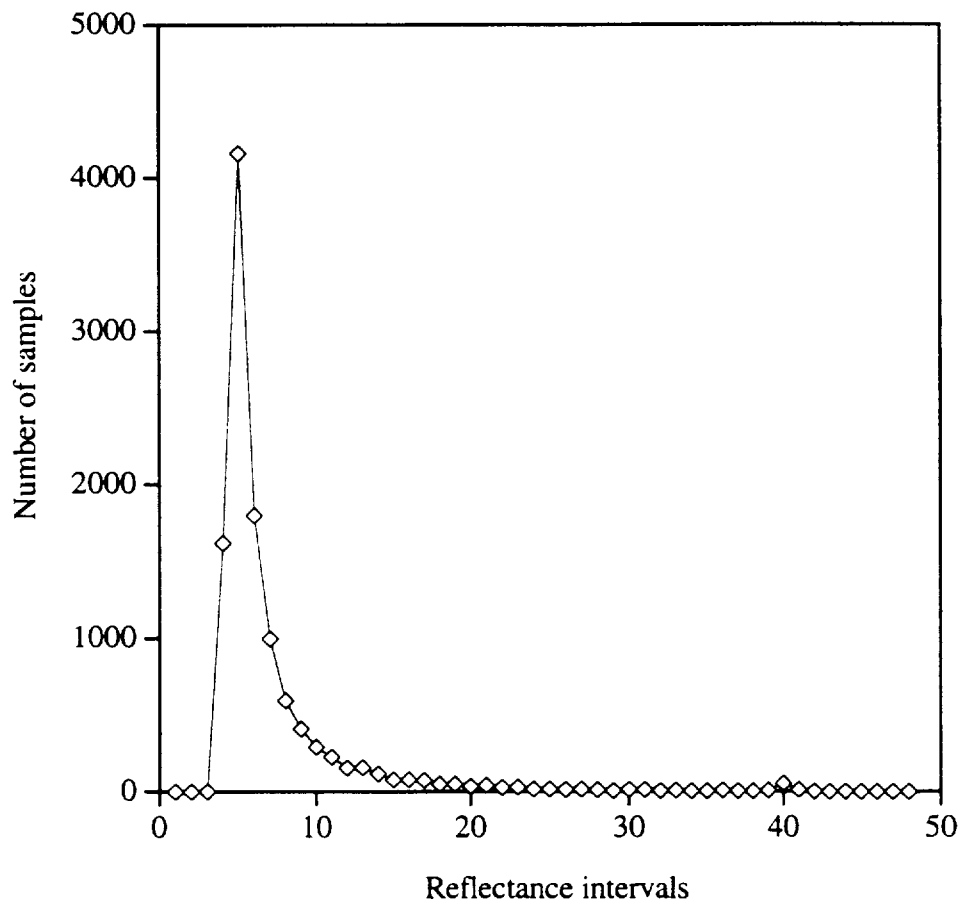


Fig. 4(b).

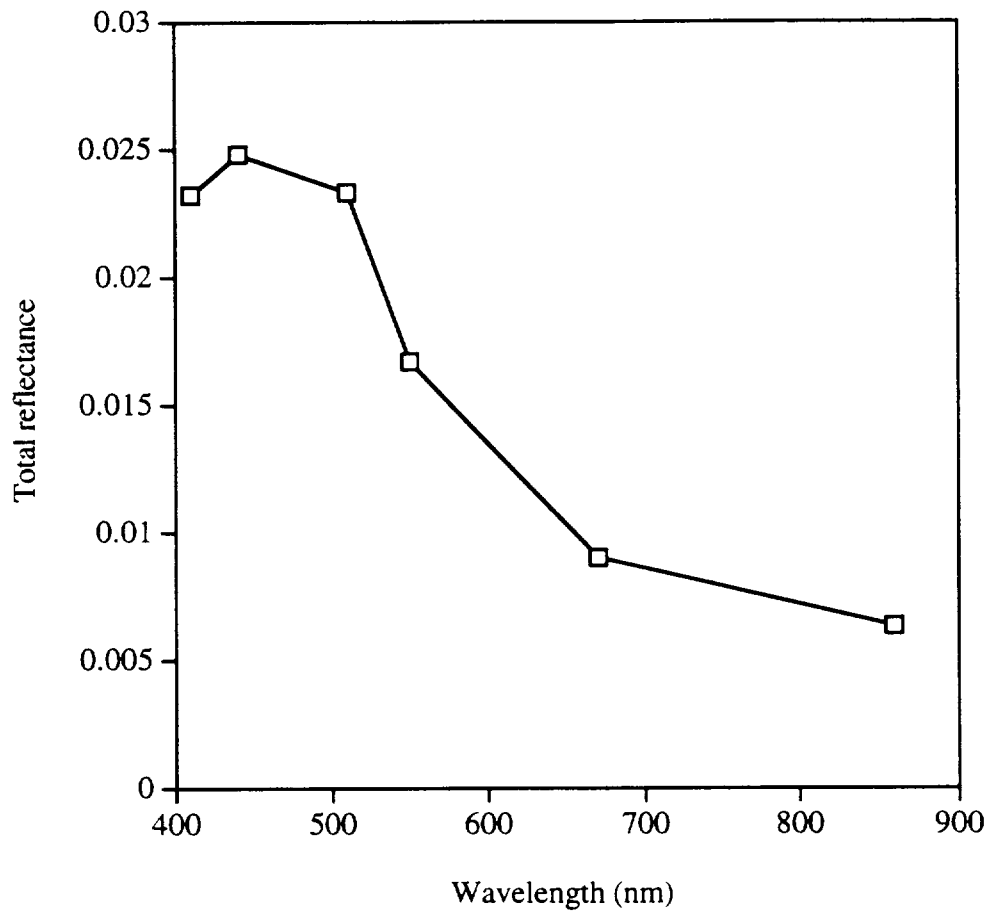


Fig. 4(c).

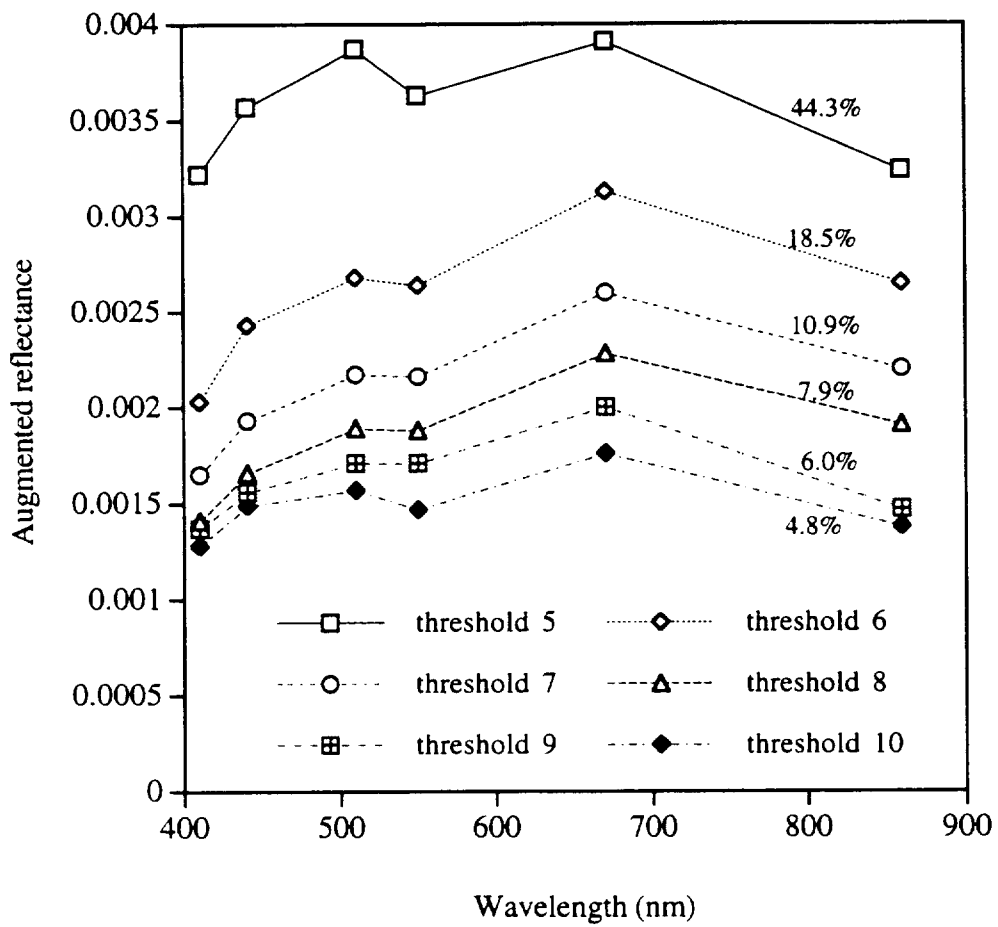


Fig. 4(d).

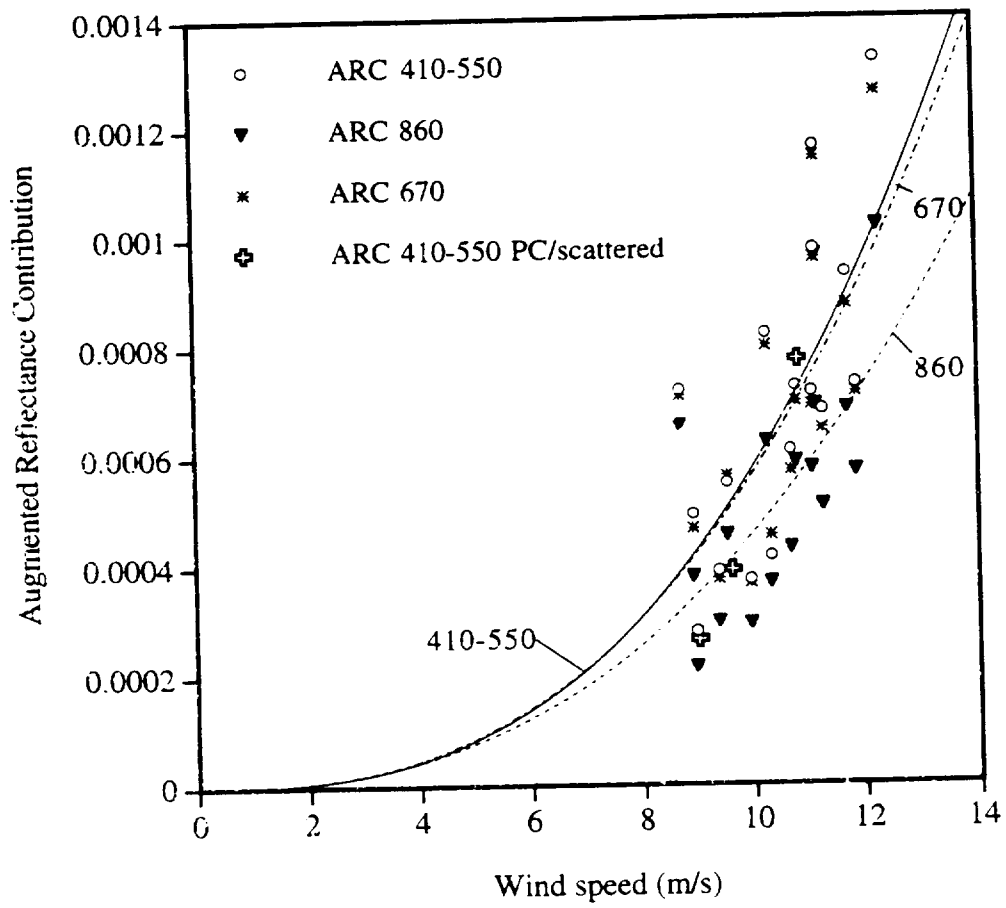


Fig. 5.

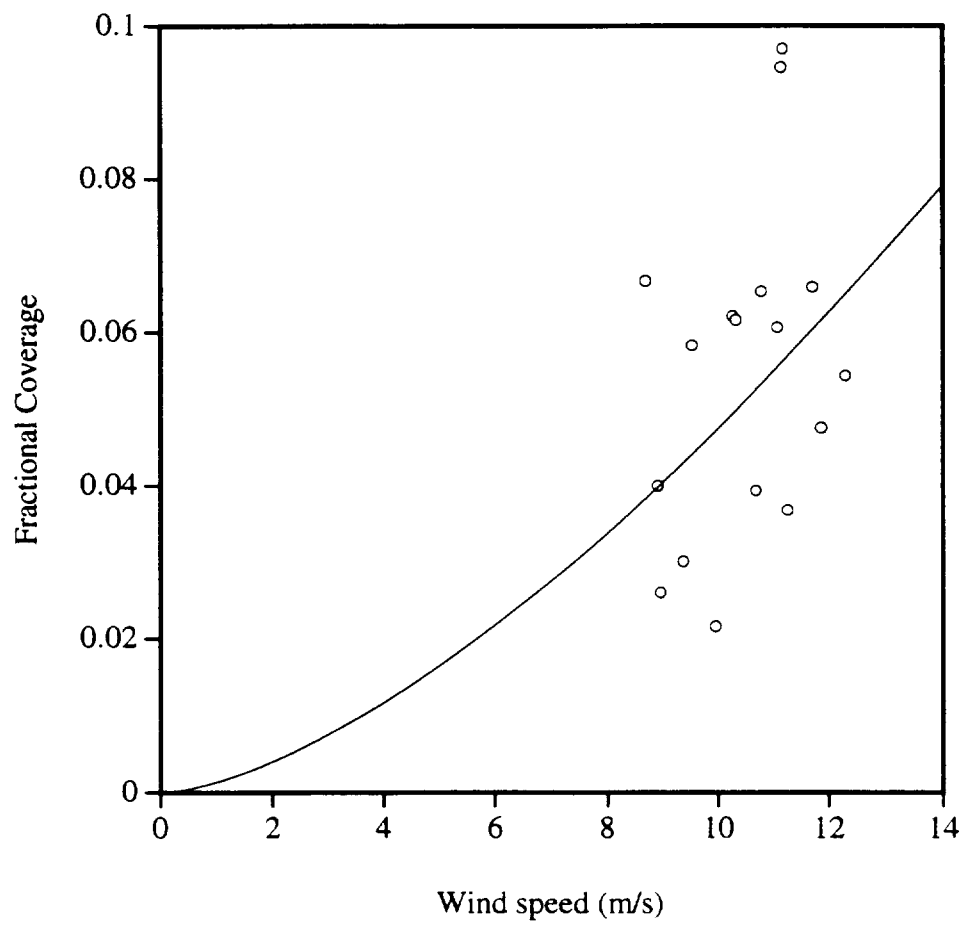


Fig. 6.

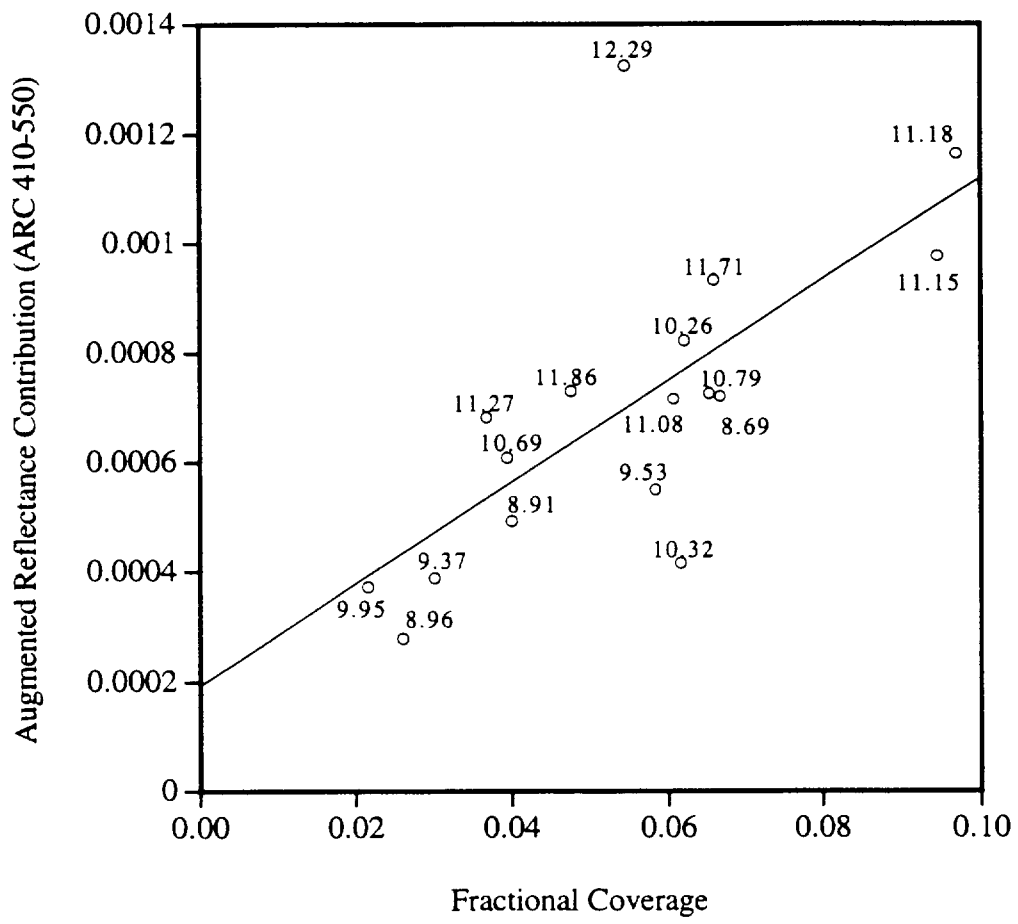


Fig. 7.

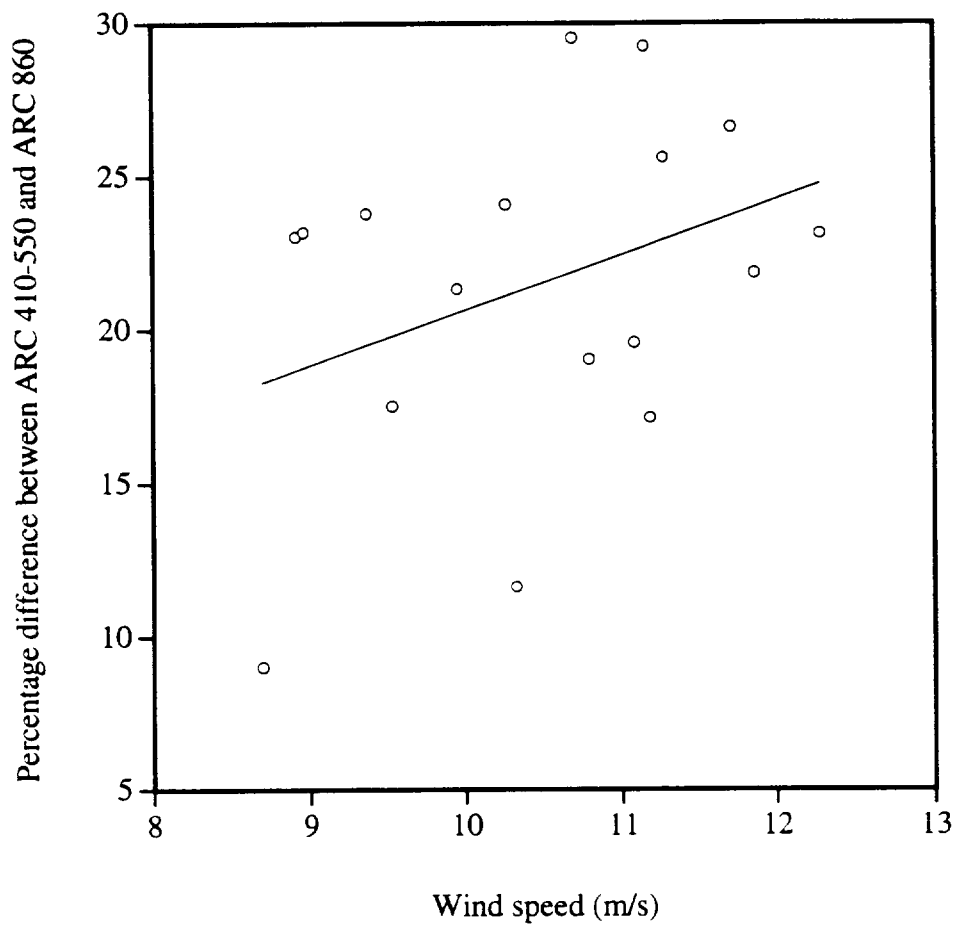


Fig. 8.

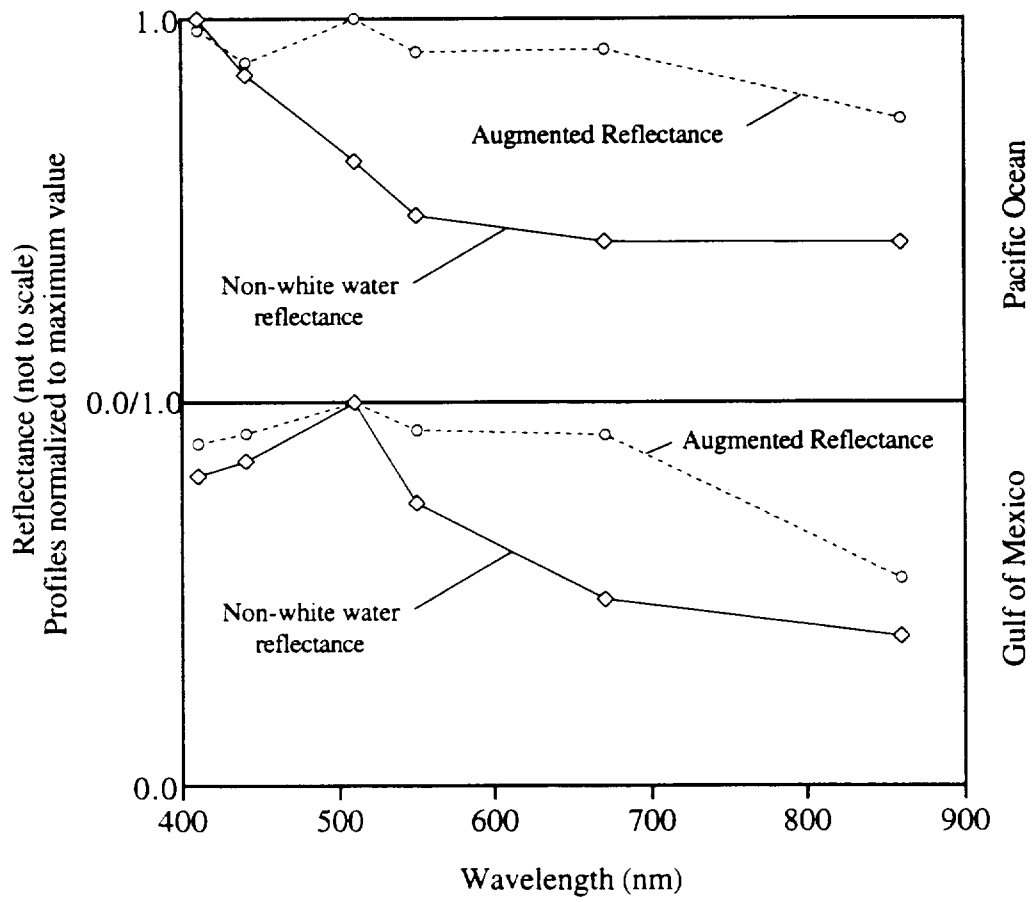


Fig. 9.